Environ Earth Sci (2017) 76:343
DOI 10.1007/s12665-017-6659-9

THEMATIC ISSUE

Geothermal potential evaluation and development prioritization based on geochemistry of geothermal waters from Kangding area, western Sichuan, China

Ji Luo[1,2] · Zhonghe Pang[1,2] · Yankong Kong[1,2] · Yingchun Wang[1,2]

Received: 10 February 2017 / Accepted: 22 April 2017 / Published online: 8 May 2017

Abstract Kangding geothermal area is located in the western Sichuan, belonging to southeastern margin of Tibetan Plateau. Similar to world-renowned south Tibetan and western Yunnan geothermal belt, western Sichuan has intensive surface thermal manifestations including boiling and hot springs. The emerging temperature of thermal waters ranges from 47 to 79 °C with total dissolved solids lying between 899 and 2550 mg/L. δ^2H–$\delta^{18}O$ isotopes indicate a meteoric source for the thermal waters and a significant positive oxygen-18 shift in the southern region. It is suggested that southern thermal waters experienced stronger water–rock interaction and are closer to thermodynamic equilibrium, which is also proved by the water type classification. The reservoir temperature calculated by empirical and theoretical chemical thermometry is 180–225 °C for the north and 225–310 °C for the south. Evidences of hydrogeochemistry, stable isotopes, geothermometry and radiocarbon dating indicate that southern region of Kangding area shows greater geothermal potential than the northern region. In addition, based on the hydrogeochemical modeling of mineral saturation, underlying problem of scaling is likely to occur in the study area. According to the results of reservoir temperature, south Kangding sub-district has greater potential in geothermal power generation and development than northern Kangding. Therefore, further exploration and drilling work should give priority to the south Kangding area.

Keywords Geochemistry · Geothermal · Western Sichuan · China

Introduction

Kangding geothermal area is located in the western Sichuan plateau, southwestern China, which is a part of southeastern margin of Tibetan plateau and Hengduan Mountains. The average elevation is over 3000 m. Intensive uplifting effect of the Tibetan Plateau resulting from collision between Indian plate and Eurasian plate leads to the formation of large-scale active strike-slip faults in western Sichuan district (Xu et al. 2011). Western Sichuan plateau is one of the regions with strongest seismic activity in mainland China. '5.12' Wenchuan Earthquake recorded 8.0 magnitude happened in the Longmenshan active thrusting strike-slip fault zone.

Western Sichuan has strong high-temperature surface thermal manifestation. As one of the most important thermal spring areas in China, there occurs 248 spring from 20 to 80 °C, accounting for 86 percent of the total in Sichuan Province (Luo 1994). Boiling and hot springs show a zonal distribution along three main large-scale strike-slip fault zones: Jinshajiang fault zone, Ganzi-Litang fault zone, and Xianshuihe fault zone. Kangding geothermal area is located along Xianshuihe fault zone, which is one of the major left-lateral strike-slip faults.

This article is part of a Topical Collection in Environmental Earth Sciences on "Subsurface Energy Storage II", guest edited by Zhonghe Pang, Yanlong Kong, Haibing Shao, and Olaf Kolditz.

✉ Zhonghe Pang
z.pang@mail.iggcas.ac.cn

[1] Key Laboratory of Shale Gas and Geoengineering, Institute of Geology and Geophysics, Chinese Academy of Sciences, No. 19, Beituchengxilu, Chaoyang District, Beijing 100029, China

[2] University of Chinese Academy of Sciences, Beijing 100029, China

In recent years, several geothermal exploration and exploitation projects have been launched in Kangding with an aim of geothermal power generation. From north to south, multiple hot spring groups occur along fault zone in Kangding area, forming a more than 10 km band zone. The springs are used for bathing, swimming, and medical purposes. Previous studies have investigated the hydrogeological and isotopic properties of hot springs in western Sichuan and Kangding (Cao et al. 2006; Chen 2014; Chen et al. 2015; Liu 2011; Luo 1994; Shen 2007; Wei et al. 2012). During the process of geothermal fluids ascending from a geothermal reservoir, hot waters may cool by mixing in the upflow with shallow groundwater (Arnorsson 2000). The mixing usually dilutes geothermal fluids and may mislead the calculation of reservoir temperatures and evaluation of geothermal prospect (Kong et al. 2014).

In this study, we have attempted to evaluate and compare geothermal potential of both the northern and the southern regions of the Kangding area based on geochemistry geothermal waters. We have collected water samples from wells between 20 and 304 meters deep and analyzed them for chemistry and isotopes. We have made a comparative study of the north–south regions with respect reservoir temperature, scaling potential, and in particular, evaluation of geothermal potential for future exploitation and development.

Geological setting

This study was conducted in Kangding County, Sichuan Province of China (Fig. 1). Sichuan Province is located in the southeast of China. There are four types of geomorphology from east to west, which are Sichuan Basin, peripheral mountains of Sichuan Basin, southeastern mountains and western Sichuan Plateau. From western Sichuan Plateau to Sichuan Basin, the altitude varies from 4500 to 200 m. The study area is located in the West Sichuan Plateau. The average elevation is over 4000 m. The point of highest elevation in the plateau is Gongga Mountain, at 7556 m above sea level. Under the influence of terrain and monsoon circulation, western Sichuan Plateau belong to subtropical and temperate climate, where the average ambient temperature and annual precipitation are below 10 °C and 500–800 mm. Climatic vertical zoning is the most distinctive feature. River systems in western Sichuan Plateau are in parallel with mountain chains, flowing to mountain area in the south. Jinsha River system traverses the whole western Sichuan Plateau. The length of the trunk stream is 1584 km, which is the upper reaches of the Yangtze River.

Western Sichuan Plateau is located in the southeastern margin of Tibetan Plateau. Cenozoic structures in southwestern Sichuan are related to the postcollisional intercontinental deformation resulting from the India–Eurasia convergence (Wang 1998). During the late Cenozoic period, crustal fragments from the Tibetan plateau were extruded eastward (Wang 1998). Sichuan Basin represents a mechanically strong and undeformed part of the Yangtze platform, which has escaped multiple deformations that affected the surrounding regions (Burchfiel et al. 1995; Royden et al. 2008). The eastward transfer of crustal material is diverted northeast and southeast around the Sichuan Basin, accommodated by shortening on the margins of the plateau and by clockwise rotation around the eastern Himalayan syntaxis (Royden et al. 2008; Zhang et al. 2004). In southwestern Sichuan Basin, a crustal fragment which has been extruded is bounded by faults of Xianshuihe–Xiaojiang fault system and Red River fault (Wang 1998).

The Xianshuihe–Xiaojiang fault system is an extensive left-lateral fault system of at least 1400 km length, passing through four major tectonic units, the Songpan–Ganzi fold belt, the Longmen Shan thrust belt, the Yangzi platform and the South China fold and thrust belts (Allen et al. 1991; Wang 1998; Xu and Kamp 2000). The Xianshuihe fault extends for 350 km in a NW–SE direction and slips left laterally at 10–12 mm/year (Meade 2007; Xu and Kamp 2000; Zhang et al. 2004). The fault has a steep dip near the surface (70–80 °C) and a total left-lateral horizontal displacement of ~60 km (Wang 1998; Xu and Kamp 2000). At its southeastern end, the fault zone connects with the Xiaojiang fault near Shimian County. The Xianshuihe fault zone is located in Songpan–Ganzi Fold Belt which is largely underlain Triassic sedimentary strata. The Triassic sedimentary strata in Songpan–Ganzi area is ~7000 m thick and divided into five subareas: (1) Nanping area, (2) Ruoergai area, (3) Maerkang–Yajiang area, (4) Yidun-Daocheng area, (5) Jinshajiang area (Xu and Kamp 2000; Zhang and Hao 1991). The study area Kangding is located in the Maerkang–Yajiang area along Xianshuihe fault. The Lower Triassic is disconformable over the Permian limestone and consists of Bocigou and Rilagou formation. The rock types of these two formations are basal conglomerate, sandstone, siltstone, slate, and limestone lenses, which are mainly distributed in Luhuo County. The Middle Triassic is Zagunao formation which is divided into two sections. Lower Zagunao formation consists of feldspathic quartz sandstone, slate, micrite, limestone, and bioclastic. Upper Zagunao formation is composed of metamorphic quartz sandstone, feldspathic quartz sandtone, slate, limestone lenses and basal conglomerate. The Upper Triassic consists of Zhuwo, Xinduqiao, Waduo, Lianghekous, and Yajiang formation. The main rock types are metamorphic feldspathic quartz sandstone, siltstone, slate, phyllite, limestone lenses, and metamorphic sandstone (Chang 2000; Su et al. 2006; Zhang and Hao 1991). To the west of Xianshuihe fault in Kangding, Precambrian and Paleozoic rocks are

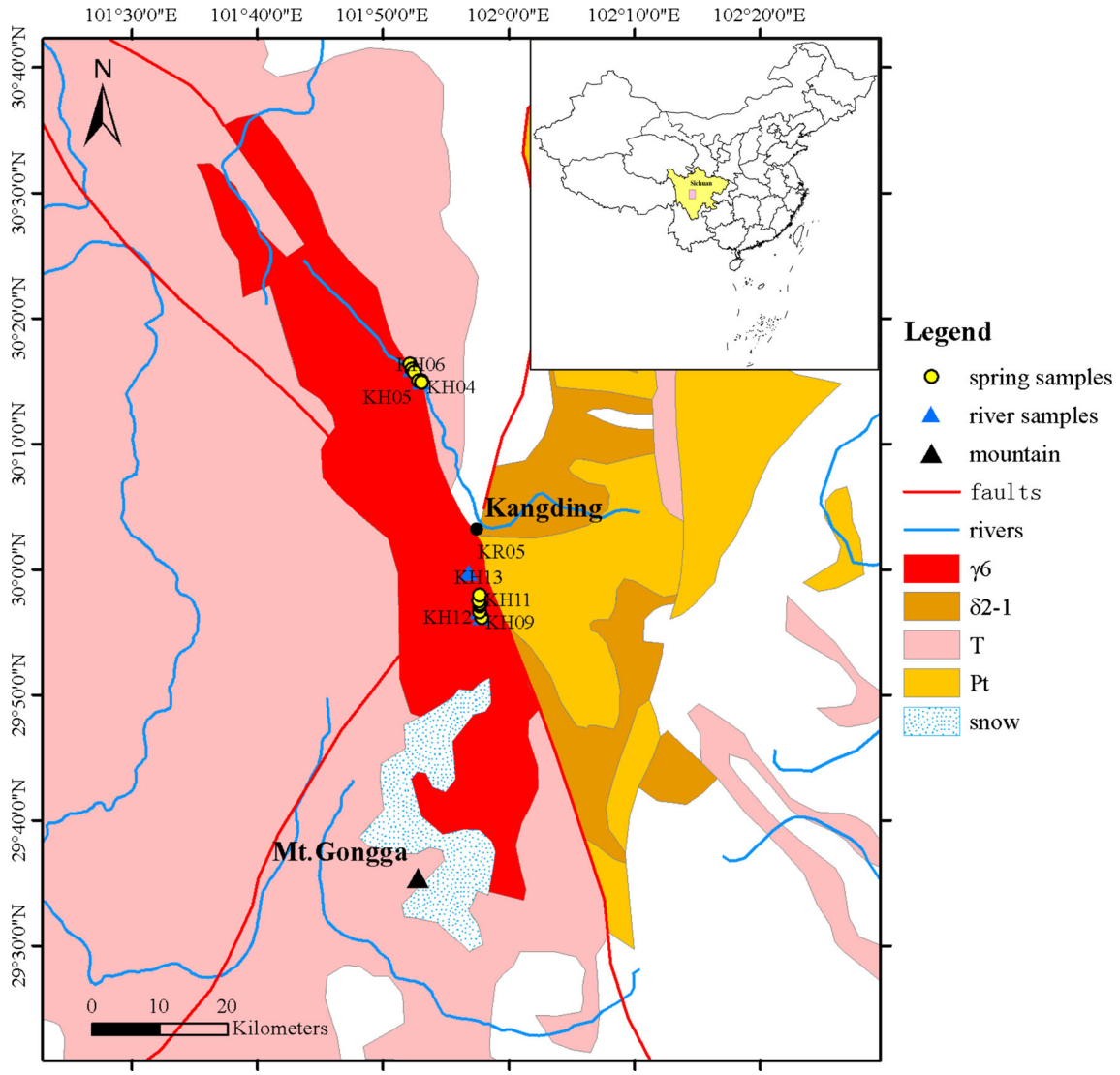

Fig. 1 Simplified geological maps and sampling locations in Kangding geothermal area (*γ6* Himalayan intrusive rocks, *δ2-1* proterozoic intrusive rocks, *T* triassic, *Pt* proterozoic)

almost exclusively underlain by Triassic sedimentary or igneous rocks (Burchfiel et al. 1995). While in the East of Xianshuihe fault in Kangding, there occurs a belt of Precambrian and Paleozoic crystalline rocks and Precambrian reoverlain along a thrust contact with Sinian and Paleozoic metasedimentary rocks (Burchfiel et al. 1995; Wang 1998; Xu and Kamp 2000). The Precambrian rocks are divided into pre-Sinian and Sinian rocks (Zhang and Hao 1991). Pre-Sinian rock types are metamorphic rocks and plutonic rocks, which are unconformably overlain by Sinian rock. The Sinian rocks are sedimentary, volcanic rocks, and marine sedimentary rocks (Zhang and Hao 1991).

There are three groups of intrusive rocks along the Xianshuihe fault zone (Xu and Kamp 2000). The oldest group of monzonitic granite and plagiogranite occurs east of the Xianshuihe Fault near Luding overlaying by Sinian strata (600–800 Ma). The second group of monzonitic granite, granodiorite, quartz monzodiorite, and diorite occurs in the central segment of the fault zone ranging from ~110 to ~210 Ma. The third group of batholith occurs along southeastern segment of the fault zone with a granite emplacement age of 13–10 Ma (Roger et al. 1995; Wang 1998; Xu and Kamp 2000). This Cenozoic large granitic pluton trending along the Xianshuihe fault near Kangding is called Gongga Shan Granite and covers an area of ~760 km^2. The study of fission track thermochronology shows that the cooling process, consisting of magmatic cooling within the upper crust and cooling via denudation, was synchronous with its deformation along the Xianshuihe Fault. Temperature related to emplacement of the granite may have reached ~240 °C under the influence 6-km radius (Xu and Kamp 2000).

Sampling and analysis

To characterize the hydrogeochemistry of geothermal waters in Kangding geothermal area, water samples from natural thermal springs, geothermal wells, and river waters were collected in August 2013 for major anion, cation, minor, and trace element, δ^2H, $\delta^{18}O$, ^{14}C analyses. A total of 13 geothermal water and 5 surface water samples were collected. Geothermal waters and surface waters were collected from two groups geographically in northern and southern Kangding. The sampling locations are shown in Fig. 2. Samples were stored in high-density polyethylene bottles which were rinsed with waters to be collected before sampling. For cation analysis, reagent-grade HNO3 was added to on sample collected at each site to bring the pH below 1. Field parameters, including total dissolved solids (TDS), electrical conductivity (EC), temperature, and pH, were measured in site by using a Senslon156 multiparameter device (made by Hach company). Stable water isotope composition was measured at the Water Isotopes and Water–Rock Interaction Laboratory, Institute of Geology and Geophysics, Chinese Academy of Sciences on a laser absorption water isotope spectrometer analyzer (Picarro L1102-i). The results were reported with respect to the Vienna Standard Mean Ocean Water (VSMOW) in ‰ with precisions of ±0.5% and ±0.2% for δ^2H and $\delta^{18}O$, respectively. The analysis of water chemistry was conducted at the Analytical Laboratory of Beijing Research Institute of Uranium Geology, where anions (F^-, Cl^-, SO_4^{2-}, NO_3^-) and cations (Ca^{2+}, Mg^{2+}, Na^+, K^+) were measured with a DIONEX-500 ion chromatograph, minor and trace element with NexION300D ICP/MS (inductively coupled plasma mass spectrometry), and alkalinity (HCO_3^-, CO_3^{2-}) using an automatic titrator METROHM^{TM}. The methods for

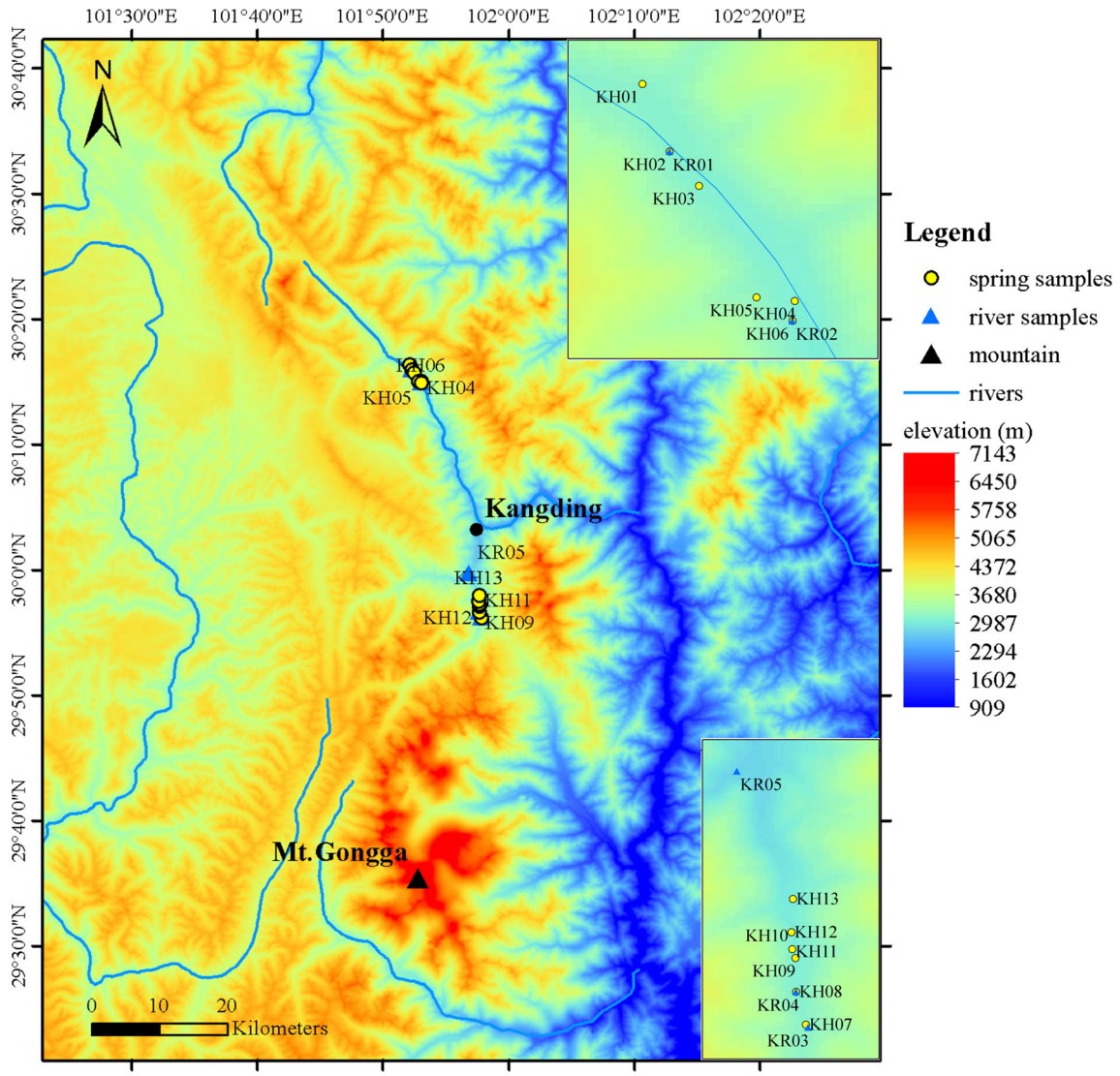

Fig. 2 Digital elevation model (DEM) and sampling location in Kangding geothermal area

cation measurements are taken from the National Analysis Standard DZ/T0064.28-1993, for anions from DZ/T0064.51-1993, for minor and trace element from DZ/T0064.80-1993 and for alkalinity from DZ/T0064.29-1993. The analytical precision was 3% of concentration based on reproducibility of samples and standards. The detection limit was 0.05, 0.1 mg/L, and 0.002 μg/L for cations/anions, HCO_3^-/CO_3^{2-}, and trace elements, respectively. The accuracy was 0.01, 0.1 mg/L, and 0.001 μg/L for cations/anions, HCO_3^-/CO_3^{2-} and trace elements, respectively. The water analyses are generally of high analytical accuracy and the charge balance error ranges from −5 to 5% for all samples. ^{14}C concentrations were measured with service of Beta Analytic Inc. (Florida, USA) on an accelerator mass spectrometry (AMS).

Results and discussion

Hydrochemistry

The results for field parameters and chemical analyses of water samples are shown in Tables 1 and 2, respectively. As shown in the sampling locations (Fig. 2), samples of KH01–KH06, KR01 and KR02 are collected along Yala River in the northern Kangding, belonging to Dagaicun, Zhonggucun, and Reshuitang geothermal fields. Samples of KH07–KH13 and KR03–KH05 are located along Yulin River in the southern Kangding, belonging to Liuhuanggou, Yulinhe and Baiyangwan geothermal fields. Natural spring samples are slightly acidic while well and river samples are slightly alkalic. Surface temperature of geothermal waters varies from 47 to 79 °C. As the boiling point of water in 3000 m above the sea level is 91 °C, geothermal waters from Dagaicun, Liuhuangou, and Yulinhe are close to boiling. Electrical conductivity values for thermal waters range from 2.88 to 10.58 mS/cm. Thermal waters are enriched in Na with respect to river waters. HCO_3 is of the main anions for both thermal and river waters. For hot waters, magnesium concentrations are lower than that of calcium and sodium, which could be explained by ion-exchange reactions occurring between magnesium, calcium, and sodium. With HCO_3–Na and Cl–HCO_3–Na as the major water types, geothermal waters have high TDS ranging from 933 to 2540 mg/L. River waters are characterized with of HCO_3–Ca and HCO_3–

Table 1 Field characteristics of water samples from two geothermal fields (temperature in °C, EC in μS/cm, TDS in mg/L and depth in meters)

Sample	Type	Depth	Location	T^a	pH[b]	EC[c]	TDS[d]	Water type
KH01	Well	20	Dagaicun	74.4	7.05	3220	955	HCO_3–Na
KH02	Spring	–	Zhonggucun	51.3	6.62	2920	933	HCO_3–Na
KH03	Well	105	Zhonggucun	58.6	7.01	3220	935	HCO_3–Na
KH04	Well	20	Reshuitang	58.3	6.63	3430	1007	HCO_3–Na
KH05	Spring	–	Reshuitang	56.9	6.56	3590	1066	HCO_3–Na
KH06	Spring	–	Reshuitang	46.9	7.12	2880	988	HCO_3–Na
KH07	Well	248	Liuhuanggou	74.0	7.51	8960	2250	Cl–HCO_3–Na
KH08	Well	305	Yulinhe	78.9	8.05	9660	2310	Cl–HCO_3–Na
KH09	Spring	–	Yulinhe	76.9	6.97	4630	1083	Cl–HCO_3–Na
KH10	Well	109	Yulinhe	79.3	8.74	10,580	2540	Cl–HCO_3–Na
KH11	Well	267	Yulinhe	68.2	8.97	8960	2500	Cl–HCO_3–Na
KH12	Spring	–	Yulinhe	58.2	6.61	3080	899	HCO_3–Na
KH13	Well	250	Baiyangwan	61.5	7.64	8090	2370	Cl–HCO_3–Na
KR01	River	–	Zhonggucun	12.8	8.00	93.9	58.1	HCO_3–Ca
KR02	River	–	Reshuitang	13.1	7.14	112.0	69.4	HCO_3–Ca
KR03	River	–	Liuhuanggou	9.9	8.02	58.6	39.4	HCO_3–SO_4–Ca
KR04	River	–	Yulinhe	12.9	8.25	88.2	53.3	HCO_3–SO_4–Ca
KR05	River	–	Zheduohe	12.2	8.51	–	–	HCO_3–Ca–Mg

[a] The accuracy of T is 0.1 °C

[b] The accuracy of pH is 0.01 pH is automatically corrected at 25 °C

[c] The accuracy of EC is 0.1 μS/cm and 0.01 mS/cm when EC is between 20.0–199.9 μS/cm and 2.00–19.99 mS/cm, respectively. EC is automatically corrected at 25 °C

[d] The accuracy of TDS is 0.1, 1 and 0.01 mg/L when TDS is between 0.00–199.9, 200–1999 and 2.00–19.99 g/L, respectively. TDS is derived from EC which is corrected with 25 °C as reference temperature and 2%/°C as linear temperature correction factor

Table 2 Chemical and isotopic analyses of waters samples from two geothermal fields (cations, anions, SiO_2 and TDS in mg/L, trace elements in μg/L, isotopic ratio in ‰ relative to the international VSMOW standard)

Sample	HCO_3^-	CO_3^{2-}	Cl^-	SO_4^{2-}	Ca^{2+}	Mg^{2+}	Na^+	K^+	TDS[a]	Li	Sr	SiO_2[b]	$\delta^{18}O$	δ^2H
KH01	876.0	0.0	70.70	2.37	19.40	24.80	282.00	26.20	863	1652.000	730.000	216	−16.81	−126.6
KH02	907.0	0.0	77.50	1.50	33.00	13.50	310.00	30.10	919	1991.000	958.000	262	−16.88	−127.6
KH03	901.0	0.0	65.10	0.44	41.10	24.80	271.00	24.30	877	1633.000	795.000	255	−16.73	−125.5
KH04	1022.0	0.0	82.40	1.28	49.50	17.40	333.00	30.40	1025	1980.000	979.000	282	−17.32	−130.3
KH05	1055.0	0.0	86.60	1.72	48.90	17.40	352.00	32.70	1067	2131.000	1110.000	280	−17.25	−130.5
KH06	973.0	0.0	74.60	0.71	33.60	20.20	312.00	28.40	956	1932.000	975.000	263	−16.77	−128.1
KH07	1351.0	0.0	655.00	6.08	11.40	3.79	867.00	108.00	2327	8285.000	1320.000	503	−16.47	−142.1
KH08	1125.0	67.2	726.00	3.73	7.10	1.99	868.00	118.00	2355	8680.000	378.000	718	−14.76	−136.7
KH09	732.0	0.0	238.00	47.70	33.50	14.70	343.00	40.80	1084	3327.000	1100.000	402	−15.60	−119.8
KH10	841.0	285.0	717.00	13.90	6.76	0.70	946.00	122.00	2512	8810.000	106.000	1095	−15.00	−137.7
KH11	714.0	336.0	760.00	12.20	3.86	0.45	973.00	134.00	2577	8928.000	526.000	1082	−14.70	−136.2
KH12	764.0	0.0	136.00	33.90	85.9	12.30	259.00	28.40	938	2074.000	620.000	300	−15.24	−115.9
KH13	1698.0	0.0	545.00	2.77	3.85	0.40	963.00	80.70	2445	7594.000	661.000	436	−16.02	−141.4
KR01	69.3	0.0	0.65	4.29	15.20	3.73	4.89	0.59	64	20.500	97.700	18	−16.00	−116.0
KR02	83.7	0.0	1.02	5.51	18.20	4.61	6.88	0.76	79	29.600	105.000	19	−16.03	−116.0
KR03	31.0	0.0	0.18	14.30	12.70	1.50	1.13	0.33	46	2.460	42.100	11	−16.37	−118.9
KR04	47.6	0.0	0.77	16.60	16.60	2.70	2.26	0.68	63	9.780	84.700	14	−16.42	−118.3
KR05	96.2	0.	0.25	12.60	19.90	8.78	5.31	0.44	96	10.200	107.000	26	−15.87	−115.2

[a] TDS is calculated from chemical analyses of cations and anions

[b] SiO_2 is calculated from chemical analyses of Si

SO_4–Ca types with TDS varying between 39.4 and 69.4 mg/L. SiO_2 and Li concentrations of thermal waters are generally higher than that of river waters. SiO_2 contents of geothermal waters vary between 215 and 1094 mg/L. Li concentrations for thermal waters are above 1.5 mg/L with maximum of 8.9 mg/L.

On the basis of concentrations of cations and anions, hot water samples in Kangding geothermal area can be divided into two groups. As shown in the Schoeller semilogarithmic diagram (Schoeller 1962) (Fig. 3), in accordance with spatial distribution, geothermal waters are classified into two groups which share the same signatures of spike. Samples in northern and southern Kangding possess different patterns of peaks. The first group including samples in the north has significantly higher concentrations of Ca^{2+} and Mg^{2+}. The second group of samples in the south is characterized with higher contents Na^+, Cl^-, and SO_4^{2-}. Exceptions are natural spring samples of KH09 and KH12 in the south, which are relatively close to the north group. It is probably due to mixing and dilution process in the upflow. River waters (KR01–KR05) manifest different peaks compared to geothermal waters, having Ca^{2+} and HCO_3^- peaks. Q-cluster analysis is made on all water samples using the hydrogeochemical results (Fig. 4). Seventeen compositions are selected as indices, which are TDS (Table 2), pH, Cl^-, SO_4^{2-}, NO_3^-, HCO_3^-, CO_3^{2-}, Na^+, Mg^{2+}, Ca^{2+}, K^+, F^-, Si, Sr, Li, Rb, and Cs. The

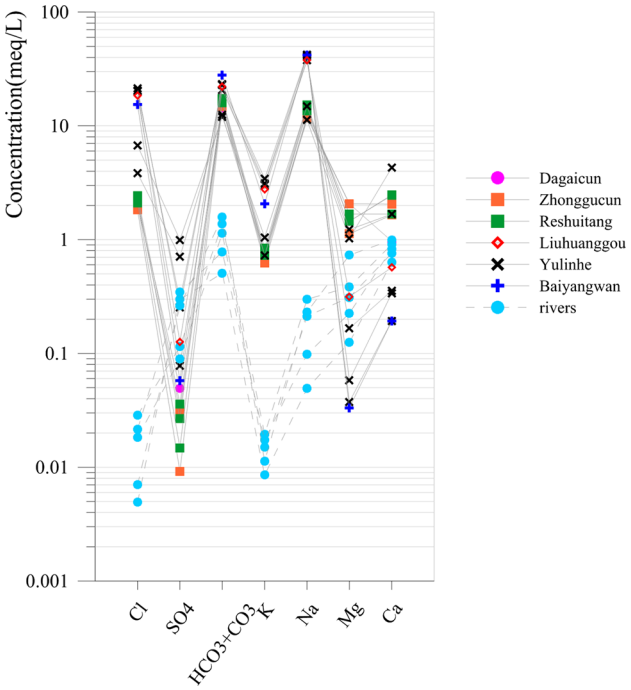

Fig. 3 Schoeller semilogarithmic diagram of geothermal water

result of statistical analysis agrees with Schoeller semilogarithmic diagram. According to the cluster results, the geothermal samples can be divided into two groups. All

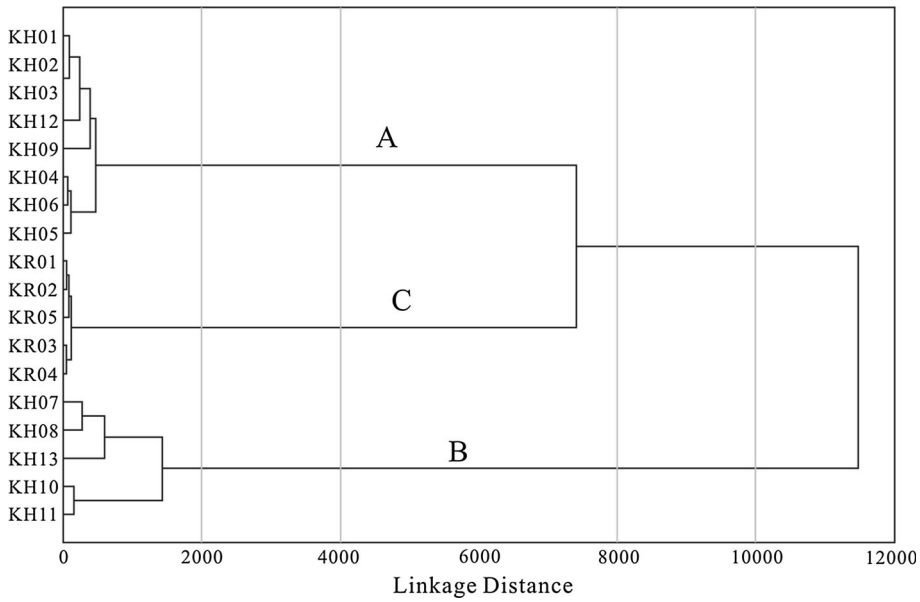

Fig. 4 Result of Q-cluster analysis of 17 hydrogeochemical indices (TDS, pH, Cl-, SO_4^{2-}, NO_3^-, HCO_3^-, CO_3^{2-}, Na^+, Mg^{2+}, Ca^{2+}, K^+, F^-, Si, Sr, Li, Rb, Cs) of all water samples

the hot water samples from the north and natural spring samples in the south (KH09 and KH12) fall into group A. Geothermal well samples from the south belong to the group C. Surface waters are divided into group B.

These two groups of thermal waters possess different hydrochemical characteristics. As shown in geological map (Fig. 1) and location of samples (Fig. 2), the first group (KH01–KH06) is collected in the boundary between Gongga granitic massif and Triassic sedimentary formation which is the main reservoir. The electrical conductivity values are between 2880 and 3590 μs/cm and are relatively dilute. The hydrochemical types are all HCO_3–Na (Table 1), having total dissolved solid (TDS in Table 2) values of 863–1067 mg/L. HCO_3 is the dominant anion with concentration between 876 and 1055 mg/L. The second group (KH07–KH13) is distributed on the Gongga granitic massif area (Fig. 2). The electrical conductivity values are between 3080 and 10,580 μs/cm and relatively saline. The waters belong almost exclusively to Cl–HCO_3–Na type with total dissolved solid (TDS in Table 2) values of 938–2577 mg/L. The primary anions are HCO_3 and Cl with contents between 714–1698 and 136–726 mg/L, respectively. Natural spring samples KH09 and KH12 are two exceptions, having lower TDS and EC among the south group. It is likely to be affected by cold shallow groundwater in the upflow. In summary, compared to samples in the south, geothermal waters from the north are relatively lower in TDS, EC, pH, and temperature. Due to the process of mixing with cold shallow groundwater, natural spring waters are relatively dilute than well waters.

A Piper triangular diagram (Piper 1944) (Fig. 5) shows that the hot waters from the north are focused in the corner of $HCO_3 + CO_3$ and Na + K. The ratio of Cl in samples is less than 10%. Both Mg and Ca account for about 10%. Samples from the southern Kangding are located in the line of Cl with an increasing tendency and a wider range between 20 and 50%. The percentage of Na is close to 100% except for KH09 and KH12. Natural spring waters KH09 and KH12 are relatively close to HCO_3 corner and possess a higher ration of Mg and Ca. In contrast to samples in the south, north group waters have an increasing proportion of Mg and Ca. Surface waters display completely different features. These samples are concentrated in Ca and HCO_3 corner, with a substantial proportion of the SO_4. According to Cl–SO_4–HCO_3 triangular diagram (Fig. 6), geothermal waters in the southern Kangding show an increasing percentage of mature water up to 50% while samples from northern Kangding are focused in the peripheral region. Increasing HCO_3 and decreasing Cl contents in geothermal waters from the north indicate increasing degree of water–rock interaction (Giggenbach and Glover 1992). The relation between (Na + K)–Cl and (Ca + Mg)–(SO_4 + HCO_3) is used to test whether cation exchange is a significant composition-controlling process (Fisher and Mullican 1997). As shown in Fig. 7, except for KH08, KH10, and KH11, thermal waters are all located along the line of $y = -x$, indicating that cation exchange controls hydrochemical features significantly. HCO_3-rich waters reflect interaction of CO_2-charged fluids at lower temperatures and migration path or mixing with shallow groundwater (Giggenbach 1991). Na-HCO_3 waters are common in geothermal systems associated with metamorphic rocks and high CO_2 content (Pasvanoğlu 2012; Vengosh et al. 2002). Rock type for reservoir in the northern Kangding is primarily Triassic metamorphous sandstone

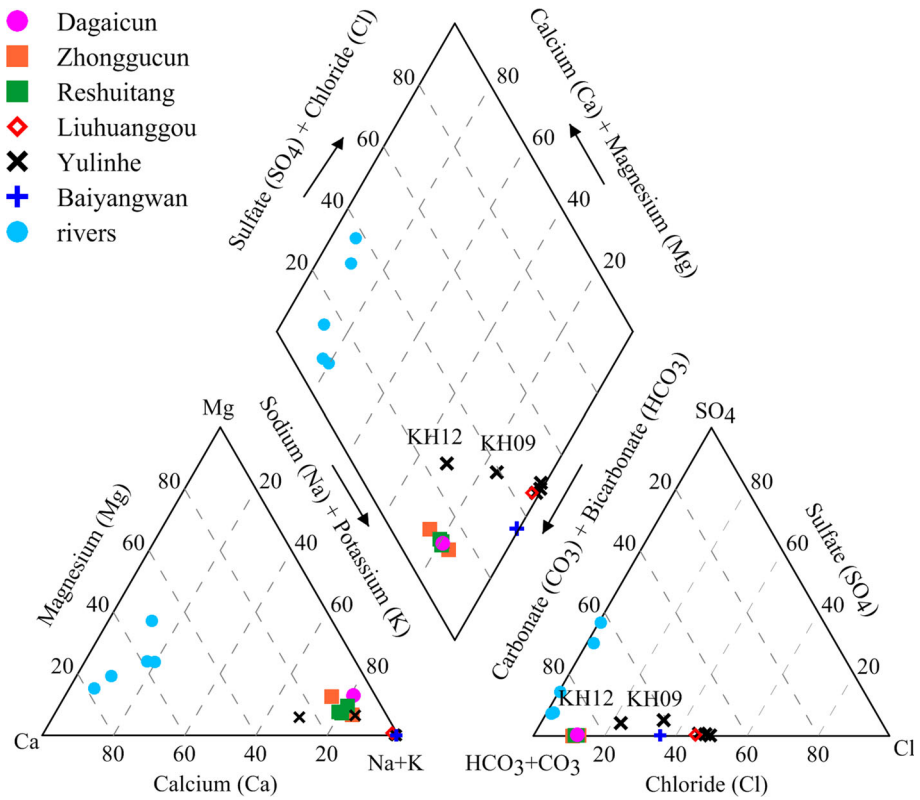

Fig. 5 Piper triangular diagram of water samples

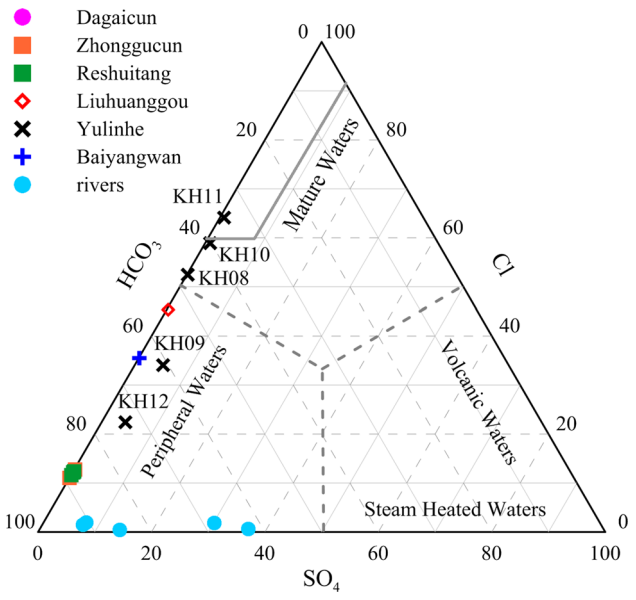

Fig. 6 $Cl–SO_4–HCO_3$ triangular diagram (Ellis et al. 1977) for geothermal samples

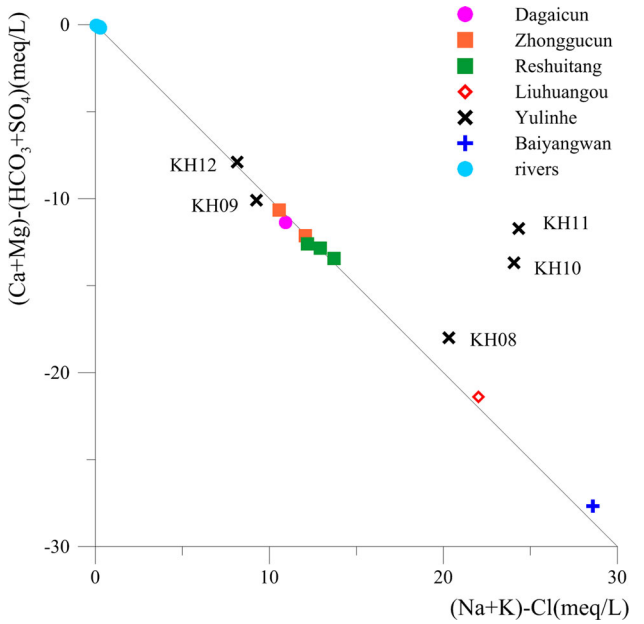

Fig. 7 Relation between (Ca + Mg)–(HCO_3 + SO_4) and (Na + K)–Cl for geothermal waters

and slate. Participation of CO_2 in water–rock reaction along migration path results in HCO_3–Na water type.

The isotopic data (Table 3; Figs. 8, 9, 10) confirmed the similar characteristics indicated by hydrochemical results. As shown in Fig. 8, geothermal waters in northern Kangding, river waters, and spring waters in southern Kangding (KH09 and KH12) are of meteoric origin. Other water samples in southern Kangding (KH07, KH08, KH10, KH11, and KH13) show different isotopic characteristics. The ^{18}O shift of second water group is remarkable. The ^{14}C apparent ages of samples are ranging from 32,400 to

Table 3 Results of carbon-14 dating for selected geothermal samples

Sample	Apparent age (BP)	pmc	pmc precision
KH01	32,400 ± 230	1.8	0.1
KH03	32,950 ± 260	1.7	0.1
KH06	34,170 ± 290	1.4	0.1
KH07	35,470 ± 330	1.2	0.1
KH10	38,680 ± 440	0.8	0.1
KH11	36,810 ± 380	1	0.1

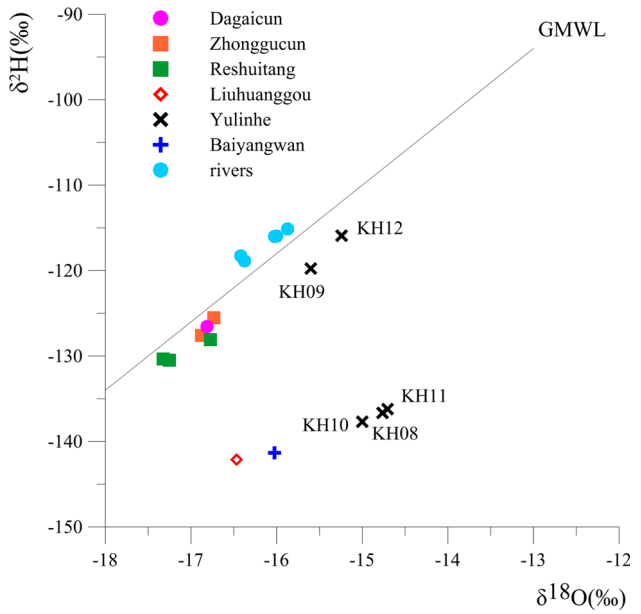

Fig. 8 Plot of $\delta^{18}O$–$\delta^{2}H$ for geothermal waters in Kangding area. GWML, global meteoric water line (Craig 1961)

38,680 BP (Table 3). Water samples in south Kangding are relatively older than north Kangding. On the basis of age, groundwater is generally classified into two groups: (1) young water or modern water (<100a); (2) old water (>1 ka). For old groundwater, approaches including ^{14}C, ^{81}Kr, $^{234}U/^{238}U$, and ^{36}Cl are used to determine the age. In this study, ^{14}C method is used for its mature technology and high efficiency. The results are within the optimum dating limit of ^{14}C method, which indicates relatively high accuracy. For KH10 and KH11, low concentration of ^{14}C ($\leq$1 pmc) may yield inaccurate and incorrect ages. In the future research, comprehensive dating approaches should be used to verify the results. Considering the fact that the measured age of water samples (Table 3) is similar, the reason for diverse isotopic features is probably due to water–rock isotope exchange. Well waters in southern Kangding experienced stronger water–rock interaction in condition of higher reservoir temperature or longer time, which are closer to thermodynamic equilibrium. It is in agreement with hydrochemical analysis (Fig. 6) and

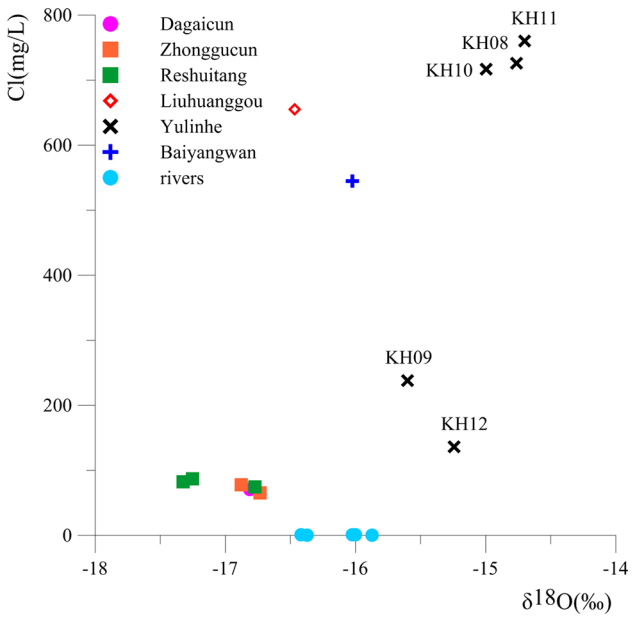

Fig. 9 Relation between $\delta^{18}O$ and Cl concentrations in water samples

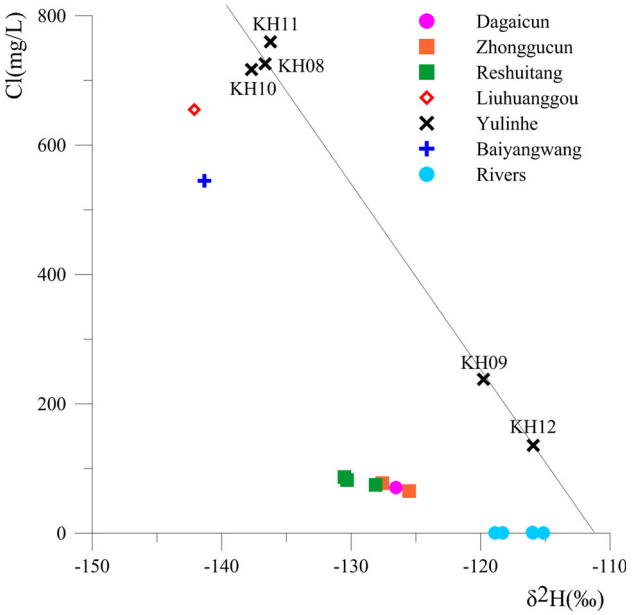

Fig. 10 Relation between $\delta^{2}H$ and Cl concentrations in water samples

geothermometer result (Fig. 12). The relation between $\delta^{18}O$ and Cl contents of thermal waters from Kangding area (Fig. 9) does not exhibit significant positive correlation. The mixing process between diverse water origins is not suggested. The relation between $\delta^{2}H$ and Cl shows the different feature (Fig. 10). Geothermal waters from Yulinhe distribute in two groups and show a linear trend when KH11, KH08 and KH10 are regarded as uniform source. The tendency equation is $y = -28.608x - 3182.5$

and R^2 is 0.99. It is assumed that KH08 represents the deep geothermal water source and intercept in x axis represents the shallow groundwater source. Based on mass-balance equation of ^{2}H and Cl, the proportions of deep geothermal fluids and shallow groundwater are calculated. The results show that KH09 is derived from 34% deep geothermal fluids and 66% shallow groundwater. The contribution of deep geothermal waters and shallow groundwaters to KH12 is 18 and 82%, respectively. The reason why δ^{18}O–Cl relation does not show the mixing trend might be that geothermal waters derived from same source experienced different degree of water–rock interaction and varied process of ^{18}O fractionation.

Recharge study is important for water resource evaluation and evaluation of aquifer vulnerability to contamination (Scanlon et al. 2002). Determining the recharge to the geothermal system is an important aspect in geothermal investigation. Geothermal fluids originated mainly from meteoric water (Craig 1963). Altitude effect of stable isotopes in meteoric water, which is induced by topographic precipitation, is useful in distinguishing groundwater recharged at high altitudes from low altitude (Blasch and Bryson 2007). The deletion of ^{18}O ranges between −0.15 and −0.5 ‰ per 100 m rise in altitude, with a corresponding decrease of about −1 to −4 ‰ for ^{2}H (Yeh et al. 2011). In this paper, the study area is located in eastern margin of Tibetan Plateau. A δ^{18}O versus elevation gradient of −0.3 ‰ (100 m)$^{-1}$ from five monitoring stations on Tibetan Plateau is used (Gao et al. 2011). Deuterium excess or d excess ($d = \delta D - 8\delta^{18}O$) is the intercept in the Global Meteoric Water Line (Craig 1961; Dansgaard 1964). A d excess versus elevation gradient of 0.12 ‰ (100 m)$^{-1}$ from the same stations is used (Gao et al. 2011). As mentioned earlier, oxygen isotope shift resulted from water–rock interaction is remarkable in the water samples. ^{2}H is used to estimate recharge area in this study. The ^{2}H-altitude slope of −2.28 ‰ (100 m)$^{-1}$ is calculated from elevation gradient of ^{18}O, d excess, and the definition of d excess. The rainy season moisture source for Kangding is believed to be the same as Chengdu. Based on GNIP database, the multiyear weighted-mean isotopic values for rainy season in Chengdu are −6.7 ‰ for ^{18}O and −49.6 ‰ for ^{2}H (Jia et al. 2008). The δ^2H values of precipitation in local area and the elevation of recharge area are calculated (Table 4). It is indicated that the recharge areas for samples in south Kangding are higher than 4300 m except for spring KH09 and KH12. The recharge area for samples in north Kangding are generally lower than 4100 m. The "recharge area" of river samples is about 3500 m, which is resulted from the mixing of precipitations and shallow groundwater in different altitudes. As KH09, KH12, and river samples share a relatively "close" recharge area, it is indicated that KH09 and KH12 experienced considerable degree of mixing with shallow groundwater in the process of upflowing, which agrees with relation between δ^2H and Cl. Moreover, as shown in Figs. 8 and 10, all samples from north Kangding are relatively close to river samples as KH09 and KH12, which increases possibility of mixing process. It is very likely that the calculated recharge elevations are lowered by mixing with shallow groundwater. Therefore, a recharge area higher than 4300 m is relatively reasonable and credible.

Table 4 The calculated elevation of recharge areas (elevation in meters, δ^2H in ‰ relative to the international VSMOW standard)

Samples	Local elevation	2H in local precipitation	Elevation of recharge area	Elevation difference
KH01	3139	−109.77	3875	736
KH02	3078	−108.38	3921	843
KH03	3066	−108.10	3829	763
KH04	3026	−107.19	4041	1015
KH05	3136	−109.70	4049	913
KH06	3019	−107.03	3943	924
KH07	3121	−109.36	4557	1436
KH08	3064	−108.06	4318	1254
KH09	3019	−107.03	3578	559
KH10	3025	−107.17	4364	1339
KH11	3025	−107.17	4300	1275
KH12	2984	−106.24	3410	426
KH13	2962	−105.73	4524	1562
KR01	3078	−108.38	3410	332
KR02	3019	−107.03	3413	394
KR03	3141	−109.81	3538	397
KR04	3064	−108.06	3513	449
KR05	2769	−101.33	3375	606

Chloride is considered as the conservative constituent for this geothermal region. The relations of the constituents in water samples from the study area are presented in Fig. 11. EC value and concentrations of SiO_2, Na, K, Mg, and Li are plotted against Cl. It is showed that samples in the first group are gathered to a rather limited extent while the second group distributing in a trend of evolution. It is likely that samples in the north share the same sources and belong to the same geothermal system. These samples are characterized with pretty similar hydrochemcical properties. In contrast, geothermal waters from the south exhibit an evolutionary trend. Except for natural spring waters (KH09 and KH12), other samples possess similar hydrochemical features. In combination of Schoeller diagram (Fig. 3), Piper diagram (Fig. 5), and relations of chemical constituents (Fig. 6), samples in the south evolve from Yulinhe, Liuhuanggou to Baiyangwan. In the plots, natural springs (KH09 and KH12) are distributed close to the first group. Considering that spring waters are commonly affected by shallow precipitation-genetic groundwater in process of upflow, geothermal waters in the northern Kangding are probably meteoric origin.

Geothermometry

For geothermal fields in the initial stage of exploitation, chemical and isotope geothermometry probably constitute the most important geochemical tool for the exploration and development of geothermal resources (Arnorsson 2000). Based on temperature-dependent water–rock equilibrium, chemical geothermometers can give the last temperature of water–rock equilibrium in the reservoir (Nicholson 2012). The reservoir temperatures in Kangding geothermal area is estimated using cation based empirical geothermometers and silica/thermodynamic equilibrium based theoretical geothermometers.

In consideration of the mixing process during ascending to the surface, some cation geothermometers may yield unreliable results. Giggenbach (1988) classified natural waters as immature, partially equilibrated or mixed and fully equilibrated on the basis of relative abundance of Na, K, and Mg concentration. The Na–K–Mg triangular diagram proposed by Giggenbach is commonly used to distinguish fully equilibrated waters from partial equilibrated waters and immature waters. Waters fall into full equilibrium line represent full water–rock reactions. Waters plotted between full equilibrium line and immature waters region are typical partially equilibrated or mixed waters. Immature waters are usually located close to Mg corner without obtaining equilibrium. In this paper, the Na–K–Mg triangle is established on the basis of Na/K (Arnórsson et al. 1983, 1998) and K/Mg geothermometers (Giggenbach 1988; Giggenbach and Soto 1992). Well waters in southern Kangding (KH07, KH08, KH10, KH11, and KH13) are all located in the partial equilibrated or mixed region (Fig. 12). It means that these waters may result from mixing between fully or partly equilibrated waters with immature waters. The distribution of data in partially equilibrated or mixed region reflects reservoir temperatures ranging from 150 to 175 °C which are significantly lower than silica geothermometers. The main reason is probably the selection of Na/K geothermometer formula. As shown in Table 5, the results of Na–K (Arnórsson et al. 1998) are remarkably lower than Na–K (Giggenbach 1988). The Na–K (Arnórsson et al. 1998)-derived triangular diagram yields relatively lower reservoir temperature. It is indicated that the selection of formulas in plotting Na–K–Mg triangular diagram determines reservoir temperature.

Data points of northern Kanding (KH01–KH06) and spring samples (KH09 and KH12) in the south fall into the region of immature waters. It is indicated that these geothermal waters have not attained equilibrium and are probably dominated by mixing with low temperature groundwater. As the cation geothermometers are based on temperature-dependent water–rock equilibrium in reservoir, cation geothermometers are not suitable for samples in immature waters. For samples in partial equilibrated or mixed field, the result of cation geothermometer is doubtful and should be considered together with silica geothermometer. Geothermal waters from southern Kangding fall into the partial equilibrated or mixed field except for KH09 and KH12. These waters experienced a higher degree of water–rock interaction with higher temperature or longer reaction time. All the geothermal samples are relatively far from full equilibrium line, indicating the unreliability of cation geothermometers.

Several chemical geothermometers are selected to evaluate the reservoir temperatures. The results of silica and cation geothermometers are listed in Table 5. Generally, the reservoir temperatures of north group are lower than south group. Located in the partial equilibrium or mixed area of Na–K–Mg diagram (Fig. 12), Na/K geothermometers are relatively reliable for these samples. Cation geothermometers producing similar results can be regarded as relatively reliable. K/Mg and Li/Mg geothermometers yield significant lower results especially for KH01–KH06. It suggests that cold groundwater rich in Mg and Ca might have mixed with deep geothermal fluids during their ascending to the surface. The relationship of Mg with other cations in geothermal waters is mainly mixing-dependent other than temperature dependent. Therefore, the K/Mg and Li/Mg geothermometers give unreliable low results. The result calculated by Na/Li geothermometer is the highest with minimum over 250 °C. The temperatures provided by silica, Na–K, and Na–K–Ca geothermometers are close and share the similar tendency,

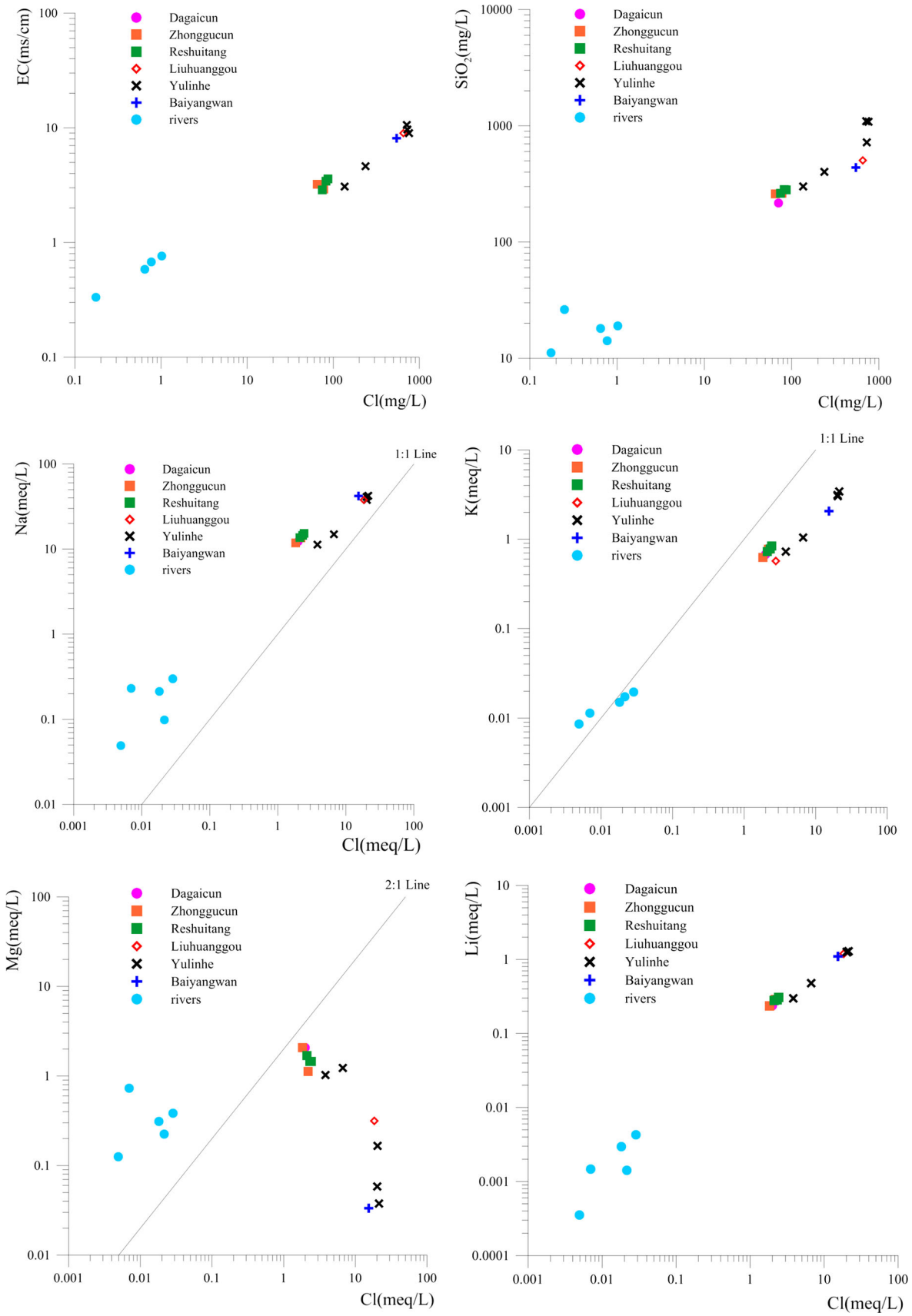

Fig. 11 Relations of chloride with EC and some chemical constituents

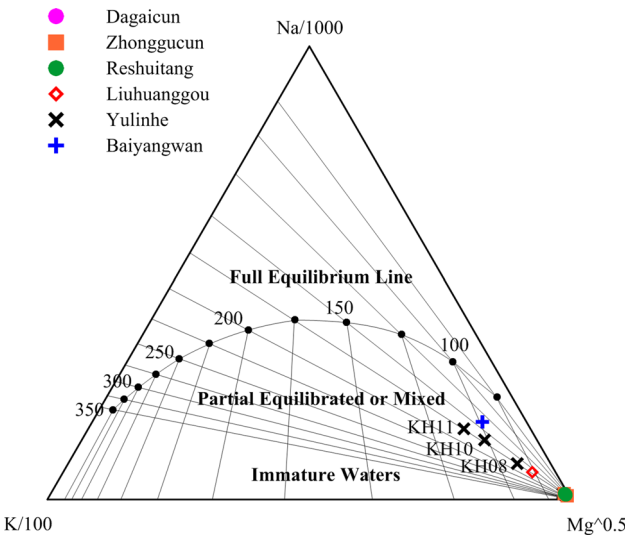

Fig. 12 Distribution of geothermal samples in Na–K–Mg triangular diagram (Arnórsson et al. 1998; Giggenbach 1988; Giggenbach and Soto 1992)

varying in a wide range of 172–335 °C. Generally, reservoir temperatures of thermal waters possess an increasing tendency toward the southern Kangding. With the highest reservoir temperatures, Liuhuanggou and Yulinhe are probably the most promising geothermal fields in Kangding. Similar temperature results for KH01–KH06 indicate that samples in northern Kangding belong to one geothermal system. With lower temperatures compared to other samples in southern Kangding, natural springs KH09 and KH12 are likely to be influenced by cold groundwater.

Another important method of chemical geothermometry is computed multicomponent chemical equilibrium in geothermal waters (Reed and Spycher 1984). By computing a group of minerals in equilibrium with each other for geothermal waters, the approach can provide good evaluation of reservoir temperature and equilibrium state when compared to conventional empirical chemical geothermometers (Pang 1988, 1991, 1992; Pang and Armmannson 1989). FixAl approach can be applied to construct a modified *Q*/*K* graph and predict reservoir temperatures for geothermal waters lacking Al or with erroneous analyses of Al (Pang and Reed 1998). By forcing the water in equilibrium with Al-containing mineral and correcting degassing/mixing process, equilibrium for a group of plausible minerals can be reconstructed, indicating the equilibrium or reservoir temperature.

With no Al content in hydrochemical analysis result for Kangding, *Q*/*K*–*T* curves of Al-containing minerals are plotted by forcing equilibrium. HCO_3-rich thermal waters in Kangding region suggest the occurring of CO_2-rich geothermal fluids and intensive degassing process in near surface. Substantial CO_2 must be added to water samples

Table 5 Calculated reservoir temperatures of samples from two different geothermal fields (in °C)

Sample	SiO_2 quartz[a]	SiO_2 quartz steam loss[a]	Na–K[b]	Na–K[c]	Na–K[d]	Na–K[e]	K–Mg[e]	Li–Mg[f]	Na–Li[g]	Na–K–Ca[h]
KH01	185	172	180	220	188	226	79	97	255	186
KH02	199	184	185	223	192	230	91	110	262	185
KH03	198	183	176	217	184	224	78	96	257	177
KH04	205	188	178	218	186	225	88	107	256	180
KH05	204	188	180	220	188	226	89	109	257	182
KH06	199	184	178	218	186	225	84	104	259	182
KH07	253	226	213	246	219	250	148	181	295	232
KH08	288	253	223	255	229	258	163	197	299	244
KH09	233	211	207	242	213	247	98	125	296	199
KH10	335	288	217	250	222	253	185	222	293	243
KH11	334	287	225	256	230	259	199	233	291	255
KH12	209	192	198	234	205	240	90	113	280	180
KH13	240	216	170	211	178	219	180	228	279	220

[a] Fournier (1977)

[b] Truesdell (1976)

[c] Fournier (1979)

[d] Arnorsson et al. (1983, 1998)

[e] Giggenbach et al. (1988)

[f] Kharaka and Mariner (1989)

[g] Kharaka et al. (1982)

[h] Fournier and Truesdell (1973)

before plotting of FixAl graphs. In this study, SOLVEQ-XPT computer program (Reed et al. 2010) is used to calculate the distribution of aqueous species and mineral saturation indices in geothermal waters. With the capability of forced mineral equilibrium and calculating pH at high temperature and pressure from low T–P–pH measurement, SOLVEQ-XPT is useful in evaluating mineral equilibria (Reed et al. 2010).

Figures 13, 14, 15, 16, 17, 18, and 19 show the original, degassing-corrected and FixAl-constructed mineral equilibria graphs of some samples in northern and southern Kangding, respectively. In original mineral distributions, talc, chrysotile, diopside, enstatite, dolomite aragonite, cristobalite, and calcite are supersaturated in whole range of temperature, indicating intensive degassing in spring vent or wellhead. Degassing is corrected by adding back same moles of component species H^+ and HCO_3^- in the input (Pang and Reed 1998), yielding approximate temperature agreement between calcite, dolomite, cristobalite, chalcedony, and quartz. The equilibria of aluminum

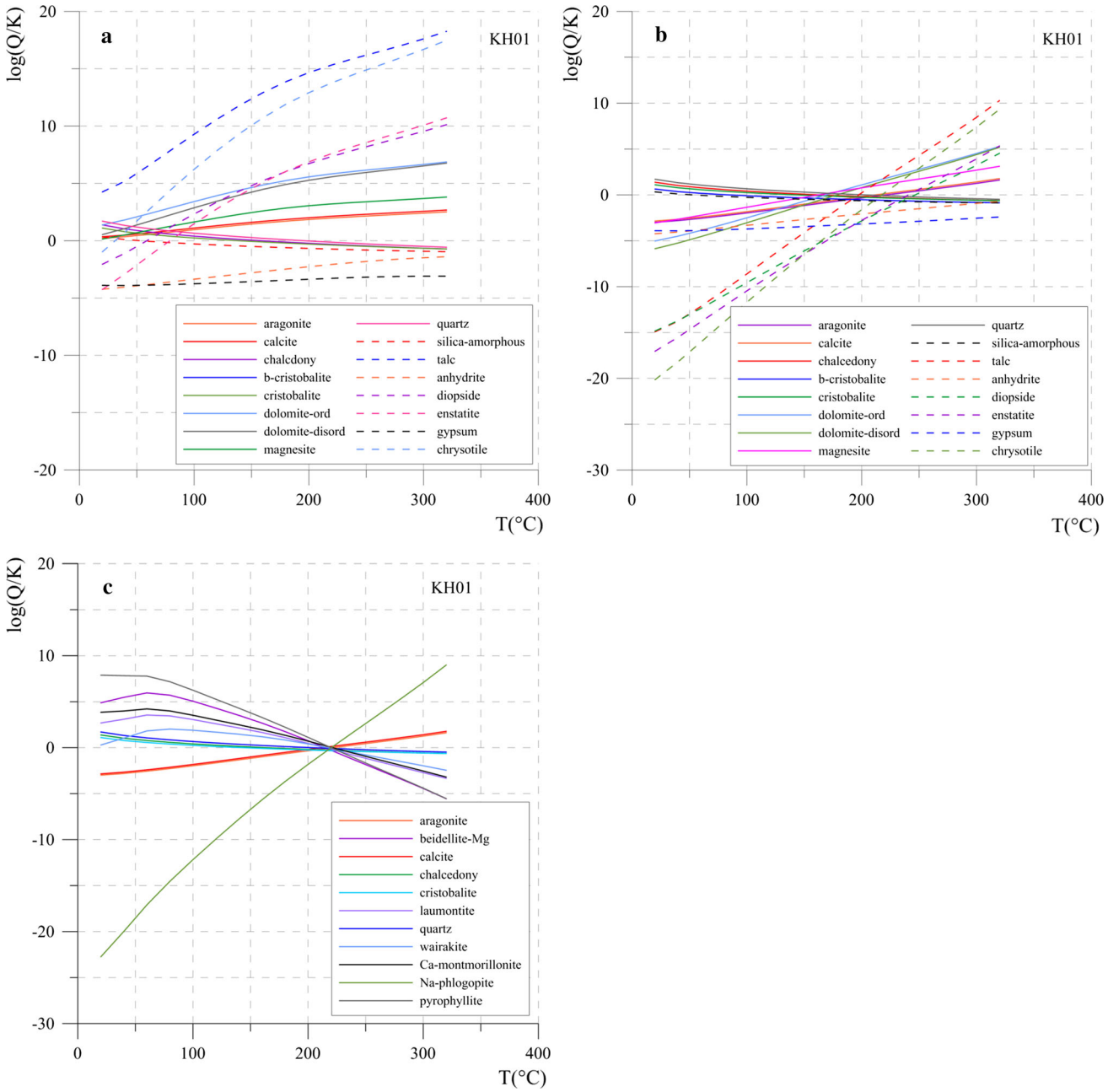

Fig. 13 Reconstructed mineral equilibria graph of KH01 (**a** original, **b** degassing and mixing corrected, **c** FixAl reconstructed)

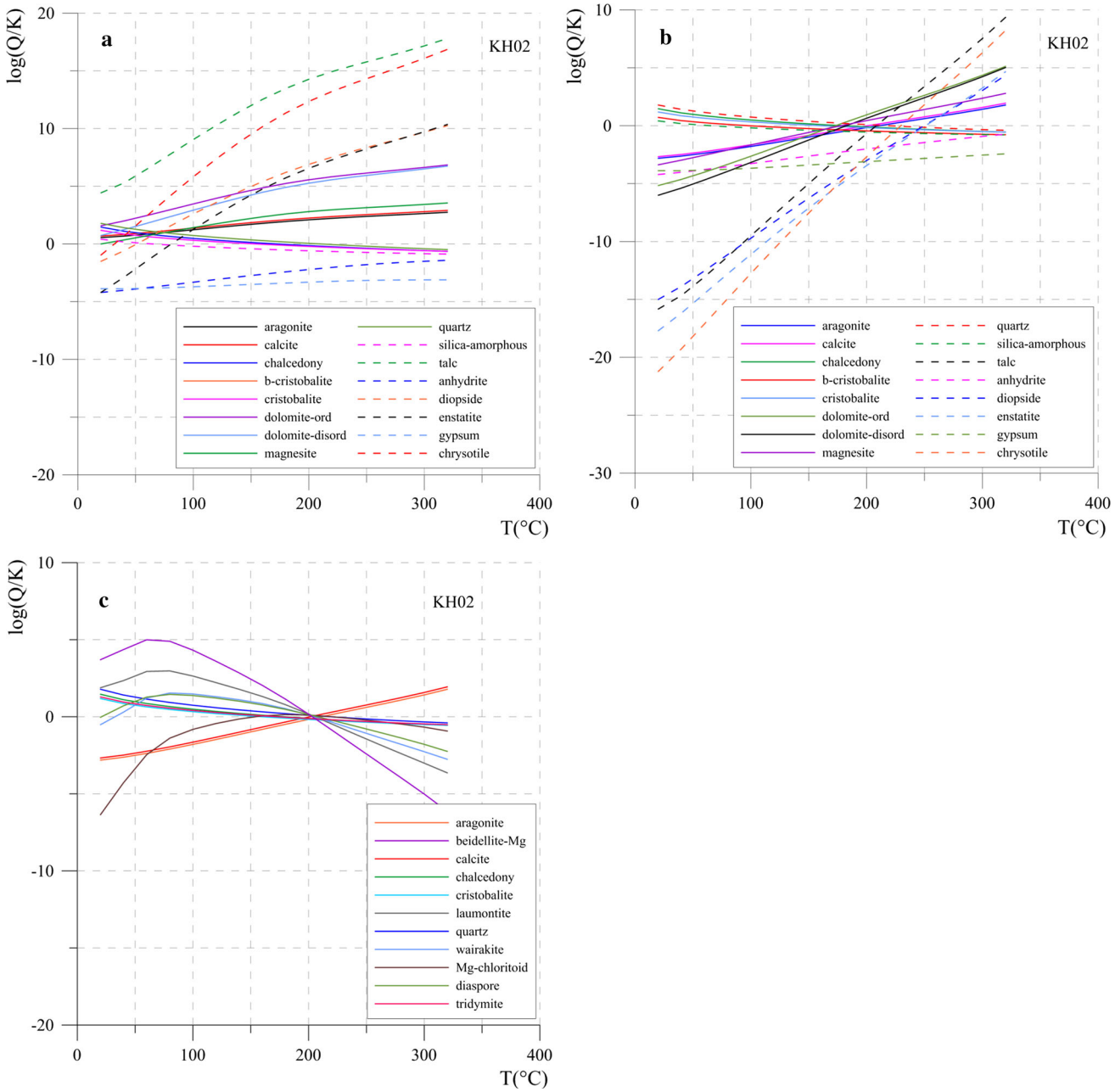

Fig. 14 Reconstructed mineral equilibria graph of KH02 (**a** original, **b** degassing and mixing corrected, **c** FixAl reconstructed)

minerals are constructed by FixAl method which selects a reasonable Al-bearing mineral for forcing equilibrium. After degassing correction and FixAl construction, a possible equilibrium temperature is yielded. The result of computed multicomponent chemical equilibrium for geothermal waters is shown in Figs. 16 and 20. The group consists of more than 10 minerals including aragonite, beidellite-Mg, beidellite-Ca, calcite, chalcedony, cristobalite, laumonite, quartz, wairakite, Mg-chloritoid, diaspore, tridymite, albite. It is shown that geothermal waters in northern Kangding (Fig. 16) have reservoir temperatures ranging between 200 and 230 °C. Samples from southern Kangding (Fig. 20) possess higher temperatures varying from 225 to 310 °C. The average reservoir temperature in northern and southern Kangding is 215 and 265 °C, respectively. Reservoir temperatures predicted by multicomponent chemical equilibrium fall into a limited range and significantly higher than silica and cation geothermometers. In the aspect of reservoir temperature, south district has greater potential in geothermal power generation and development. In future exploration and site selection, it is important to take flow capacity, steam

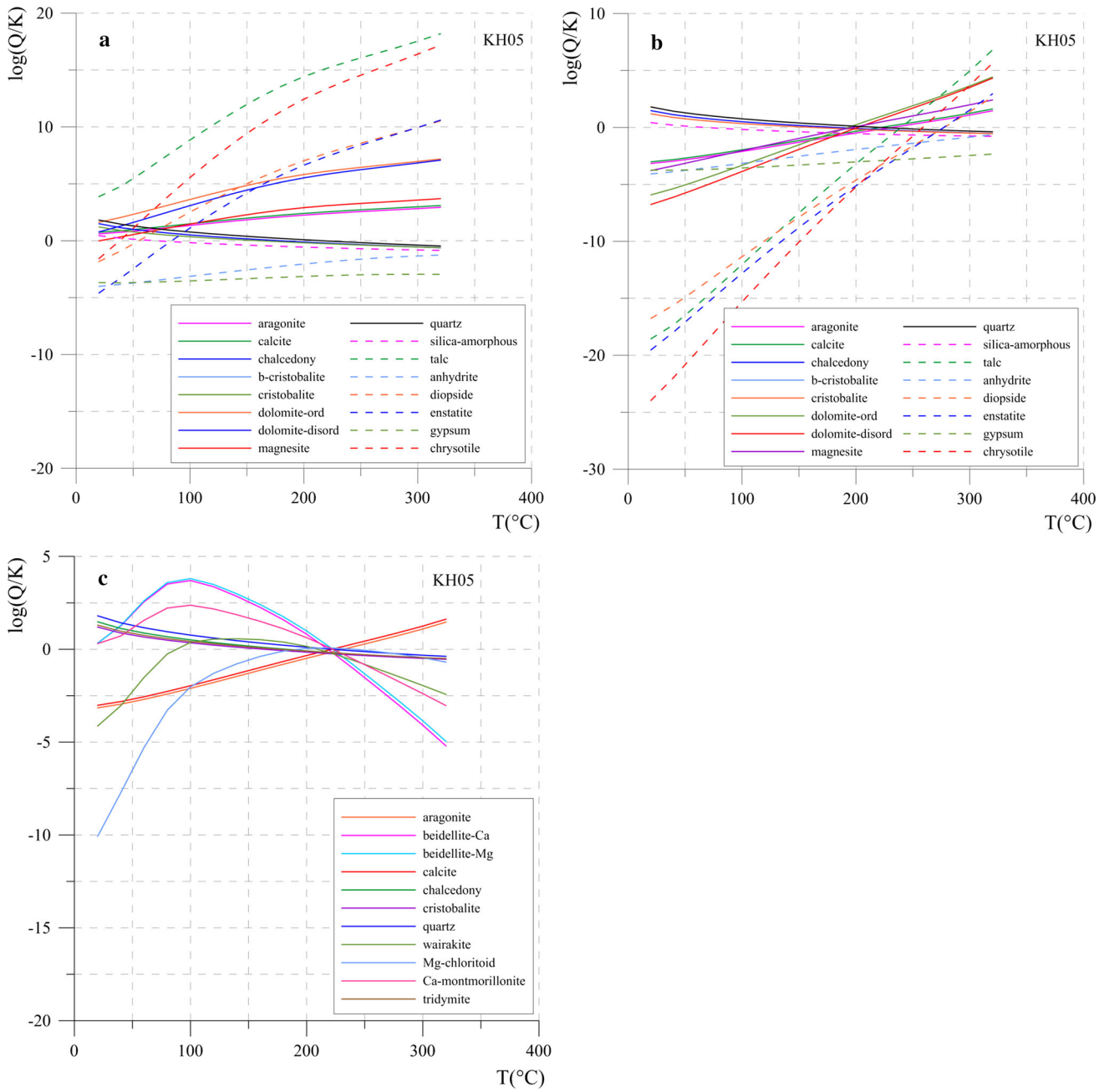

Fig. 15 Reconstructed mineral equilibria graph of KH05 (**a** original, **b** degassing and mixing corrected, **c** FixAl reconstructed)

pressure, traffic condition, and other economic factors into account.

Fig. 16 FixAl graph for reconstructing mineral equilibria and estimating equilibrium temperature for geothermal waters in northern Kangding

Mineral Saturation and Scaling Potential

Calculation of mineral saturation in geothermal waters and prediction of scaling is essential in evaluating geothermal resources for future development and utilization. Scaling is a common problem especially found in high-temperature geothermal systems. When high-temperature geothermal fluids are produced from subsurface, the changed temperature, pH, pressure, and oxidation–deoxidation environment may alter the saturation condition of minerals dissolved in geothermal waters. The degassing process due to depressurization in production wells aggravate the scaling problem especially the calcite and dolomite. Precipitation of minerals on the borehole walls, valves, and

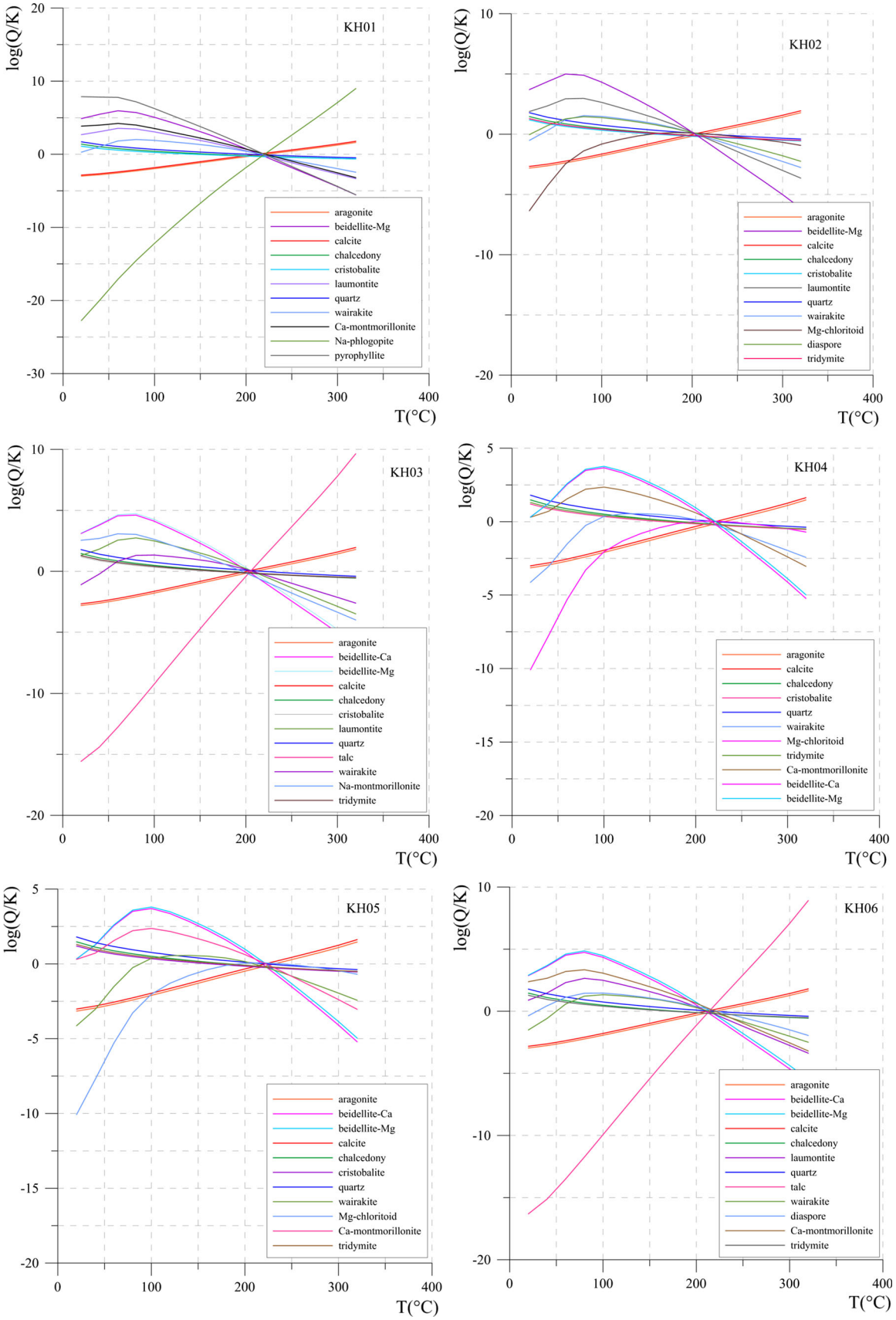
KH01
log(Q/K)
T(°C)
aragonite
beidellite-Mg
calcite
chalcedony
cristobalite
laumontite
quartz
wairakite
Ca-montmorillonite
Na-phlogopite
pyrophyllite
KH02
log(Q/K)
T(°C)
aragonite
beidellite-Mg
calcite
chalcedony
cristobalite
laumontite
quartz
wairakite
Mg-chloritoid
diaspore
tridymite
KH03
log(Q/K)
T(°C)
aragonite
beidellite-Ca
beidellite-Mg
calcite
chalcedony
cristobalite
laumontite
quartz
talc
wairakite
Na-montmorillonite
tridymite
KH04
log(Q/K)
T(°C)
aragonite
calcite
chalcedony
cristobalite
quartz
wairakite
Mg-chloritoid
tridymite
Ca-montmorillonite
beidellite-Ca
beidellite-Mg
KH05
log(Q/K)
T(°C)
aragonite
beidellite-Ca
beidellite-Mg
calcite
chalcedony
cristobalite
quartz
wairakite
Mg-chloritoid
Ca-montmorillonite
tridymite
KH06
log(Q/K)
T(°C)
aragonite
beidellite-Ca
beidellite-Mg
calcite
chalcedony
laumontite
quartz
talc
wairakite
diaspore
Ca-montmorillonite
tridymite

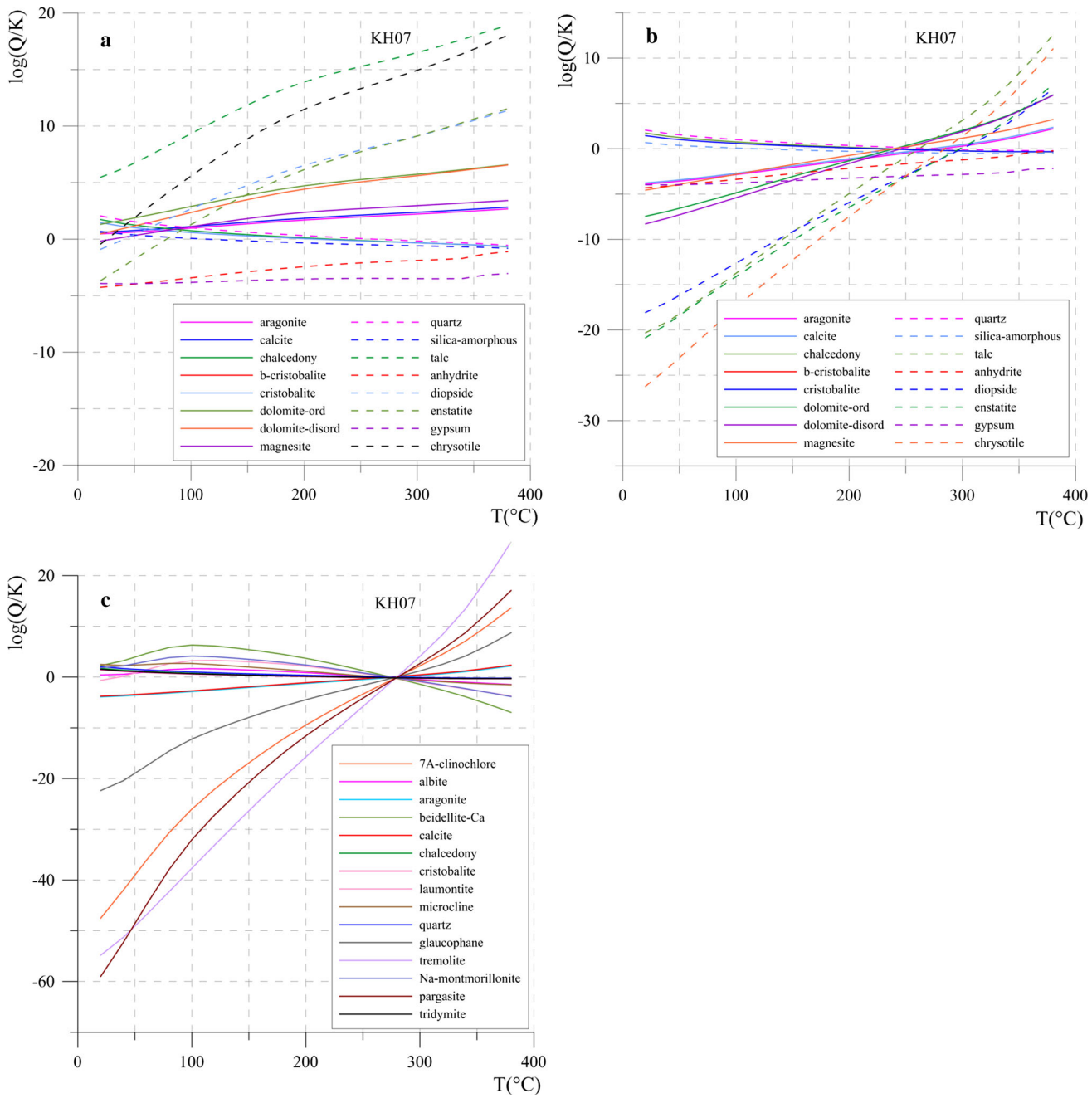

Fig. 17 Reconstructed mineral equilibria graph of KH07 (**a** original, **b** degassing and mixing corrected, **c** FixAl reconstructed)

pipelines decreases the flow rate and pressure, which severely hampers the production and utilization of geothermal fluids. Therefore, assessment of scaling potential in the initial stage of exploration is necessary. The saturation indices of carbonate (calcite, aragonite, dolomite, and others), sulfate (gypsum, anhydrite and others) and silica (quartz, chalcedony and others) minerals are helpful in scaling prediction and estimating which minerals tend to precipitate during production. When the saturation index is zero, there exists a thermodynamic equilibrium. A negative index indicates undersaturation, and a positive index indicates supersaturation. To predict minerals which may precipitate during production and development of geothermal fluids, it is important to calculate saturation index (SI) for some hydrothermal minerals.

Ryzner's index (Ryznar 1944), Larson's index (Larson and Sollo 1967), and hydrogeochemical simulation (Tarcan 2005; Wei et al. 2012; Zhang et al. 2016) are generally used to evaluate the scaling trend. In this study, the scaling tendency of geothermal waters in Kangding is evaluated

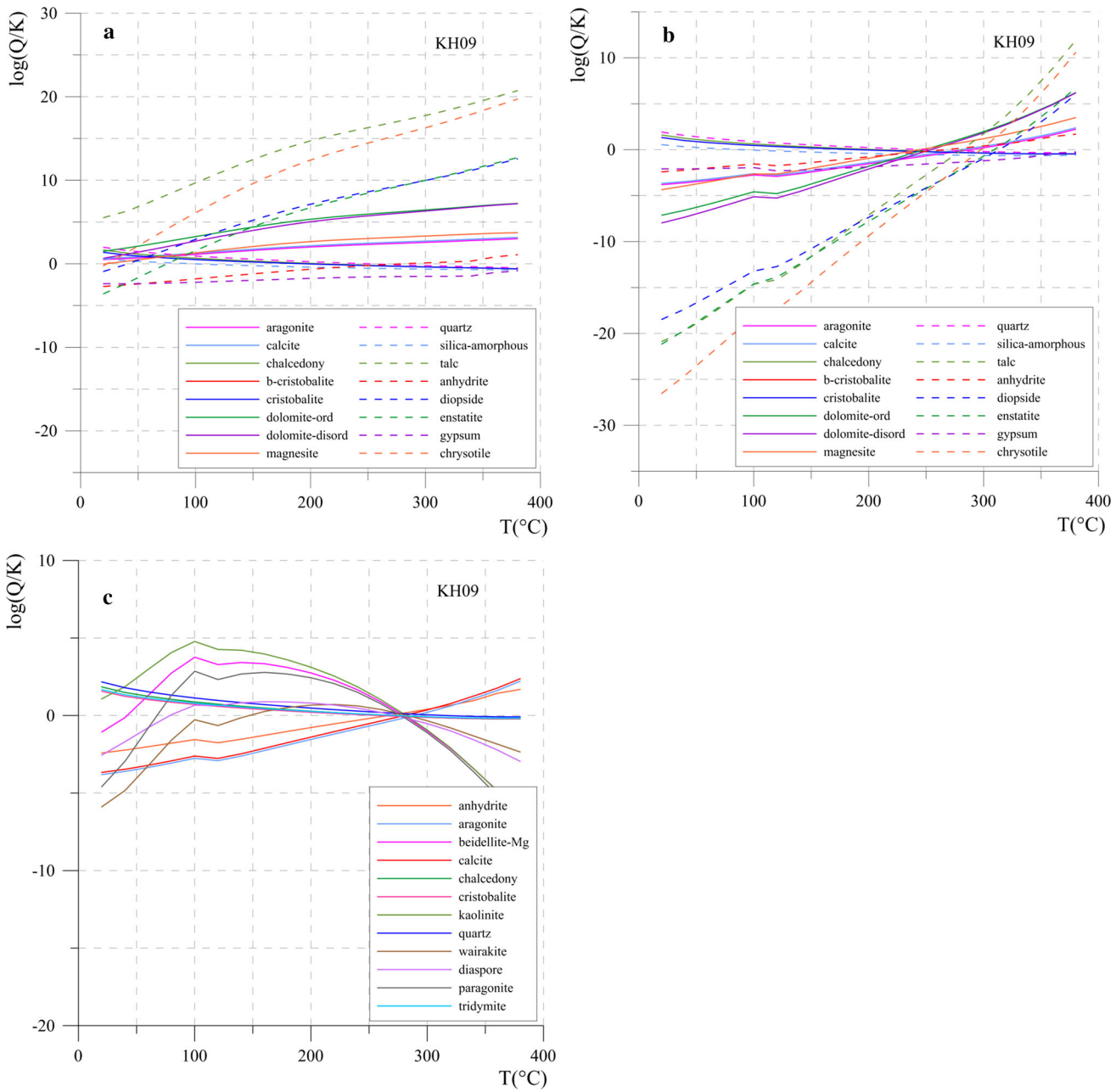

Fig. 18 Reconstructed mineral equilibria graph of KH09 (**a** original, **b** degassing and mixing corrected, **c** FixAl reconstructed)

using hydrogeochemical simulation. Mineral saturation indices are calculated for several typical hydrothermal minerals using SOLVEQ-XPT (Reed et al. 2010). The calculation of chemical equilibrium is based on laboratory analyses of hydrochemical indexes. The saturation indices (SI = log(Q/K)) of a group of hydrothermal minerals are calculated from surface measured temperature to over 300 °C by forced mineral equilibrium with Al-containing mineral and increasing temperature step by step are calculated. The mineral equilibrium diagrams of geothermal waters versus temperature are plotted in Fig. 21. As shown in the figures, calcite is almost oversaturated at each temperature for all the geothermal samples. In the mineral equilibrium diagram, aragonite and dolomite exhibit similar trend with the calcite for most water samples. Except for individual samples in northern Kangding, most samples are oversaturated with aragonite and dolomite. In contrast, most waters are undersaturated with respect to gypsum, anhydrate, albite, kaolinite, and illite minerals in near surface and reservoir. In high temperatures over 300 °C, some samples are oversaturated with gypsum, anhydrate, and albite. Scaling problems of carbonate minerals (calcite,

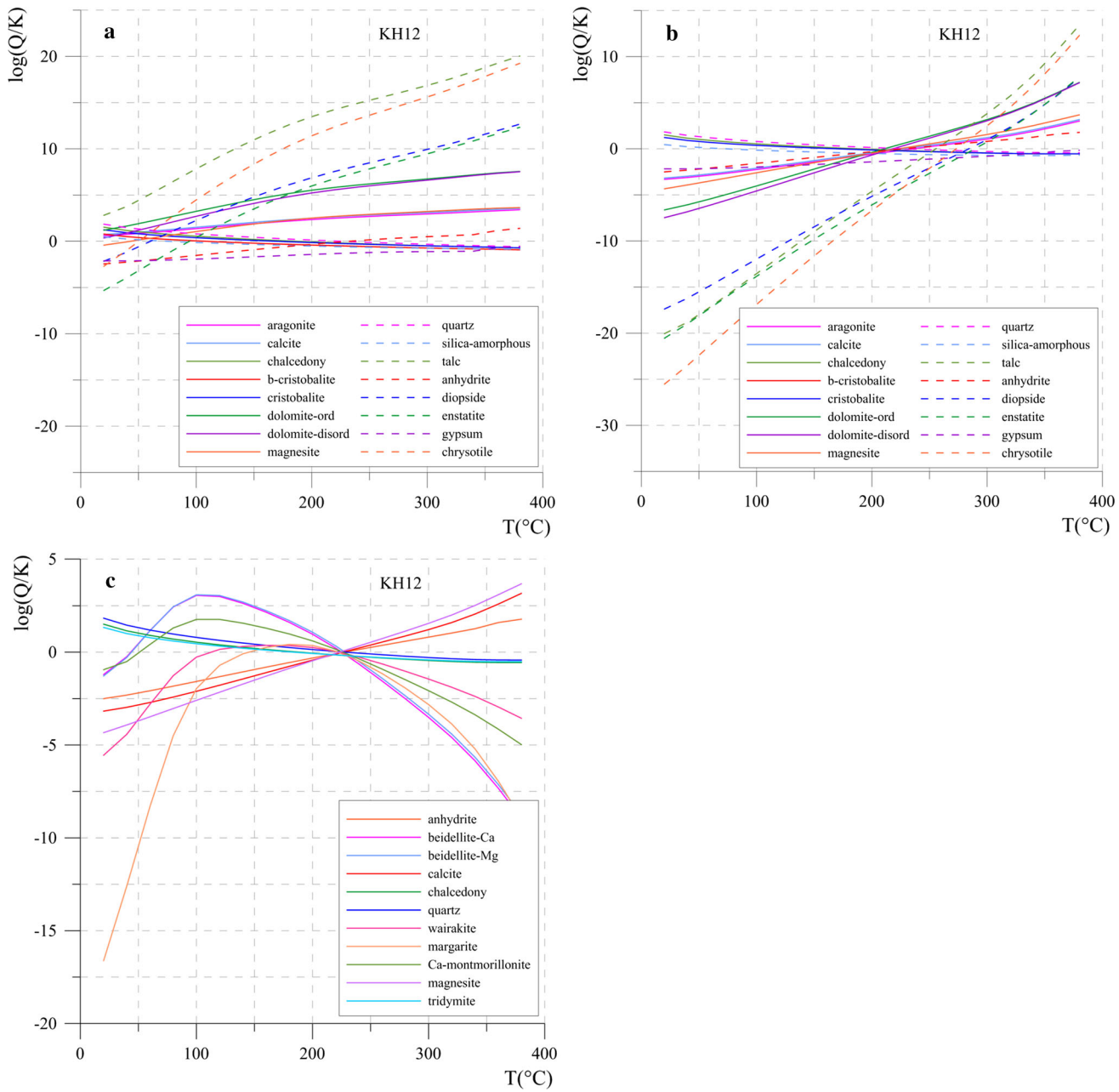

Fig. 19 Reconstructed mineral equilibria graph of KH12 (**a** original, **b** degassing and mixing corrected, **c** FixAl reconstructed)

aragonite, and dolomite) are most likely to happen in Kangding geothermal area. In addition, quartz, chalcedony and silica-amorphous may probably precipitate at lower temperatures in surface. Sulfate minerals are not likely to precipitate during exploitation and development. These results are in accordance with hydrochemical characteristics. As the main constitution in waters, substantial HCO_3 ions are probably resulted from reaction between CO_2-rich geothermal fluids and Triassic metamorphic rocks. In the future work of exploitation and development, degassing of CO_2 from high-temperature geothermal fluids may cause a certain degree of carbonate scaling in pipelines, valves, and power generation equipment. According to the results, carbonate minerals are probably the main scaling problems in Kangding geothermal area if it occurs.

The results of mineral saturation and scaling potential are in agreement with previous research and field observations (Wang et al. 2015; Wei et al. 2012; Zhang et al. 2016). A geothermal well in northern Kangding district scales seriously in the process of blow off stage and exploitation. XRD analysis showed that the main composition of scaling is calcium carbonate with 5% silica (Wang

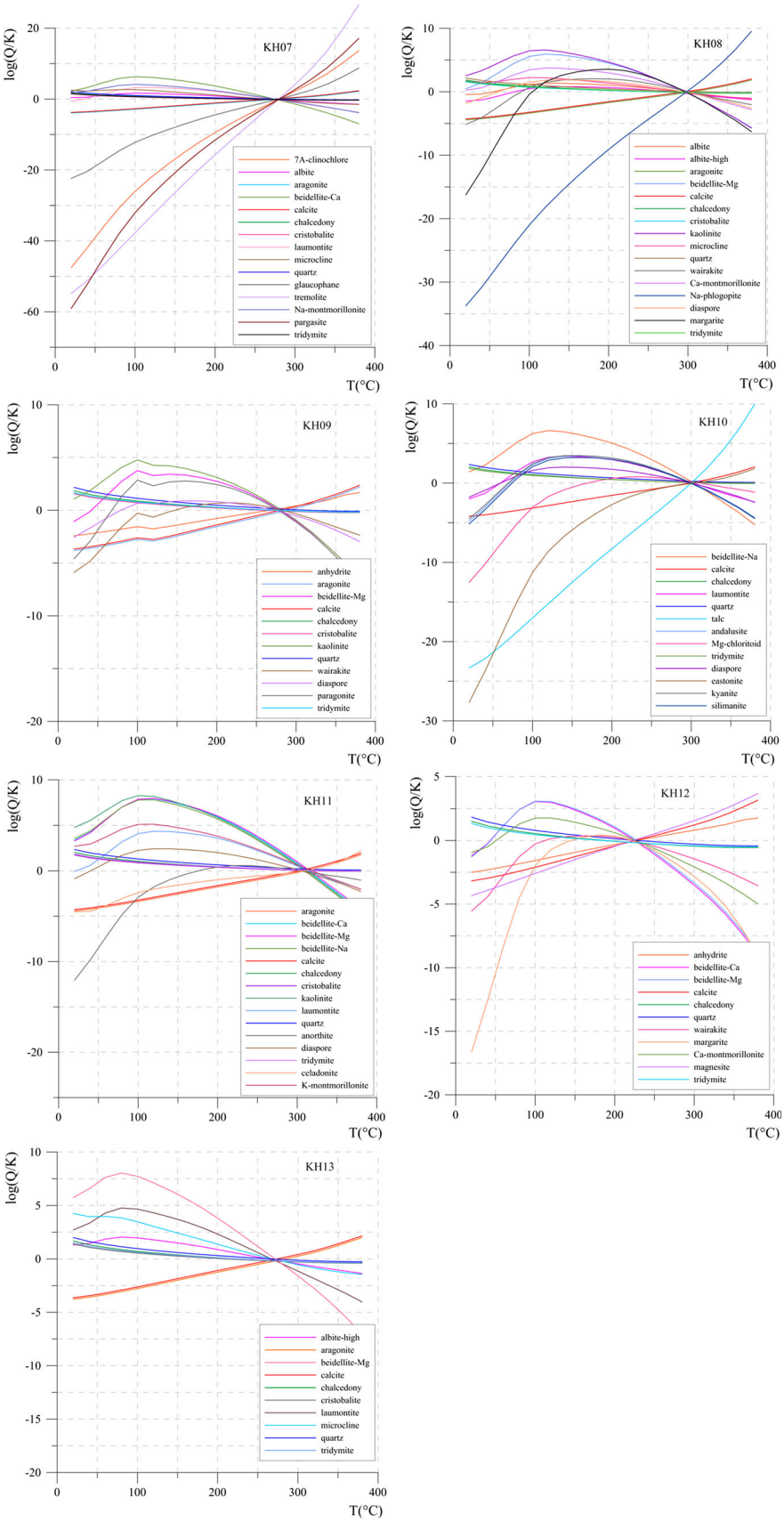

Fig. 20 FixAl graph for reconstructing mineral equilibria and estimating equilibrium temperature for geothermal waters in southern Kangding

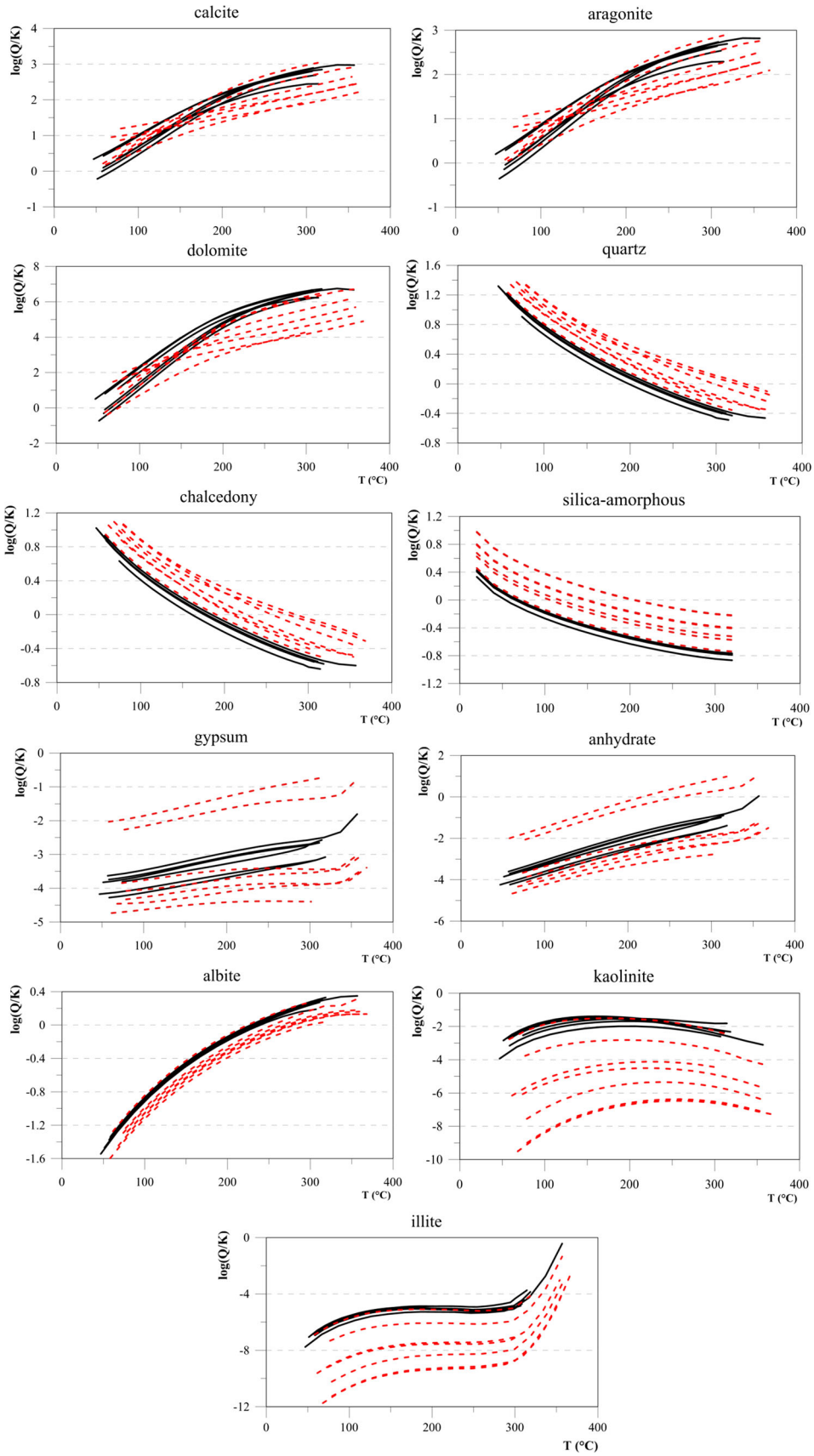

Fig. 21 Mineral equilibrium diagrams of geothermal waters (*black solid lines* represent samples from northern Kangding, *red dash lines* represent samples from southern Kangding)

et al. 2015; Zhang et al. 2016), which is in accordance with simulation results in this study. Decrease in temperature, pressure, and degassing of CO_2 during production are the primary causes of scaling problem in Kangding. There are two widely used alternatives to remove or prevent calcite precipitation in the wells. The first is to remove the scaling periodically by mechanical cleaning and acidization. The second is to inject anti-scalant in the production wells. By altering the surface of the growing crystal or chelating the calcium ions, anti-scalants can prevent the forming of calcite deposition effectively. For existing and future geothermal development projects in Kangding, application of anti-scalant is recommended to prevent scaling problem and ensure mining efficiency.

Conclusions

Kangding geothermal area in western Sichuan, China, has intensive high-temperature geothermal manifestation. The geothermal fields in Kangding can be divided into two groups in geography and hydrochemistry. The north group is HCO_3–Na type belonging to peripheral waters with ion exchange controlling the hydrochemical features. The south group is Cl–HCO_3–Na water type with remarkably higher contents of Na^+, SO_4^{2-} and an increasing trending of Cl. The TDS and electrical conductivity of south group is significantly higher than the north group. KH08, KH10, and KH12 in Yulinhe field are close to mature waters. Isotopic features and relationship between major ions indicate samples in northern Kangding are of meteoric origin, while well waters in the south experienced intensive water–rock interaction with significant positive oxygen shift.

Empirical geothermometers and silica/thermodynamic equilibrium based theoretical geothermometers are used to calculate reservoir temperatures. The results of cation and silica geothermometers range from 172 to 335 °C. Multi-component chemical equilibrium in geothermal waters is computed by SOLVEQ-XPT to calculate reservoir temperatures. Geothermal waters in northern Kangding have reservoir temperatures ranging between 200 and 230 °C. Samples from southern Kangding possess higher temperatures varying from 225 to 310 °C except for KH12.

The analysis of mineral saturation shows that most waters are oversaturated with aragonite and dolomite in both near surface and reservoir. Scaling problems of carbonate minerals are most likely to happen in Kangding geothermal area. Southern Kangding sub-district has higher reservoir temperature than north area, indicating greater potential in geothermal power generation and development. For the prospective exploration, other key indicators including but not limited to flow capacity, steam pressure, injection condition, traffic infrastructure, and economic factors should be considered together to support optimal decision making regarding priority for development.

Acknowledgements This study is supported by the National Natural Science Foundation of China (Grant 41430319).

References

Allen CR, Zhuoli L, Hong Q, Xueze W, Huawei Z, Weishi H (1991) Field study of a highly active fault zone: the Xianshuihe fault of southwestern China. Geol Soc Am Bull 103(9):1178–1199

Arnorsson S (ed) (2000) Isotopic and Chemical Techniques in Geothermal Exploration, Development and Use – Sampling Methods, Data Handling, Interpretation. International Atomic Energy Agency, Vienna, Austria, pp 351

Arnórsson S, Gunnlaugsson E, Svavarsson H (1983) The chemistry of geothermal waters in Iceland. III. Chemical geothermometry in geothermal investigations. Geochim Cosmochim Acta 47(3):567–577

Arnórsson S, Andresdottir A, Gunnarsson I, Stefánsson A (1998) New calibration for the quartz and Na/K geothermometers–valid in the range 0–350 °C. In: *Proc. geoscience society of Iceland annual meeting*, pp 42–43

Blasch KW, Bryson JR (2007) Distinguishing sources of ground water recharge by using δ^2H and $\delta^{18}O$. Ground Water 45(3):294–308

Burchfiel B, Zhiliang C, Yupinc L, Royden L (1995) Tectonics of the Longmen Shan and adjacent regions, central China. Int Geol Rev 37(8):661–735

Cao Y, Li H, Liu Z, Yuan D, Shen L (2006) Comparison of geochemical features of warm springs between Chongqing and Kangding. Carsolog Sin 25(2):112–120

Chang EZ (2000) Geology and tectonics of the Songpan–Ganzi fold belt, southwestern China. Int Geol Rev 42(9):813–831

Chen Z (2014) Hydrogeochemistry of the hot springs in western Sichuan Province, Southwestern China after the Wenchuan Ms8.0 earthquake, University of Science and Technology of China

Chen Z, Xu Y, Zheng K (2015) Geochemistry of potential high temperature geothermal resources in Kangding, Sichuan, China. Geochemistry 19:25

Craig H (1961) Isotopic variations in meteoric waters. Science 133(3465):1702–1703

Craig H (1963) The isotopic geochemistry of water and carbon in geothermal areas. In: Tongiorgi E (ed) Nuclear Geology on Geothermal Areas. Spoleto, Italy, pp 17–54

Dansgaard W (1964) Stable isotopes in precipitation. Tellus 16(4):436–468

Ellis AJ, Ellis W, Mahon W (1977) Chemistry and geothermanl systems. Academic Press, New York

Fisher RS, Mullican WF III (1997) Hydrochemical evolution of sodium-sulfate and sodium-chloride groundwater beneath the northern Chihuahuan Desert, Trans-Pecos, Texas, USA. Hydrogeol J 5(2):4–16

Fournier R (1977) Chemical geothermometers and mixing models for geothermal systems. Geothermics 5(1–4):41–50

Fournier R (1979) A revised equation for the Na/K geothermometer. Geoth Resour Counc Trans 3:221–224

Fournier R, Truesdell A (1973) An empirical Na-K-Ca geothermometer for natural waters. Geochimica et Cosmochimica Acta 37(5):1255–1275

Gao J, Masson-Delmotte V, Yao T, Tian L, Risi C, Hoffmann G (2011) Precipitation water stable isotopes in the south Tibetan Plateau: observations and modeling. J Clim 24(13):3161–3178

Giggenbach WF (1988) Geothermal solute equilibria. derivation of Na–K–Mg–Ca geoindicators. Geochim Cosmochim Acta 52(12):2749–2765

Giggenbach W (1991) Chemical techniques in geothermal exploration. Appl Geochem Geotherm Reserv Dev 11:9–144

Giggenbach W, Glover R (1992) Tectonic regime and major processes governing the chemistry of water and gas discharges from the Rotorua geothermal field, New Zealand. Geothermics 21(1–2):121–140

Giggenbach WF, Soto RC (1992) Isotopic and chemical composition of water and steam discharges from volcanic-magmatic-hydrothermal systems of the Guanacaste Geothermal Province, Costa Rica. Appl Geochem 7(4):309–332

Jia G, Wei K, Chen F, Peng PA (2008) Soil *n*-alkane δD vs. altitude gradients along Mount Gongga, China. Geochim Cosmochim Acta 72(21):5165–5174

Kharaka YK, Mariner RH (1989) Chemical geothermometers and their application to formation waters from sedimentary basins, Thermal history of sedimentary basins. Springer, pp 99–117

Kharaka YK, Lico MS, Law LM (1982) Chemical Geothermometers Applied to Formation Waters, Gulf of Mexico and California Basins: ABSTRACT. AAPG Bulletin 66(5):588–588

Kong Y, Pang Z, Shao H, Shengbiao H, Kolditz O (2014) Recent studies on hydrothermal systems in China: a review. Geothermal Energy 2:19

Larson T, Sollo FW (1967) Loss in water main carrying capacity. J Am Water Works Assoc 59(12):1565–1572

Liu Y (2011) Genesis of the geothermal water in Simaqiao-Xiaoreshui area of Kangding, Sichuan Province. Master Degree thesis, China University of Geosciences, Beijing

Luo L (1994) Inquisition of the distribution and cause of the hot springs in western Sichuan. J Chongqing Teach Coll Nat Sci Ed 11(2):39–47

Meade BJ (2007) Present-day kinematics at the India-Asia collision zone. Geology 35(1):81–84

Nicholson K (2012) Geothermal fluids: chemistry and exploration techniques. Springer Science & Business Media, Berlin

Pang Z (1988) Multiple fluid-mineral equilibrium calculations and their applications to geothermometry and hydrochemical processes in geothermal systems. Rep. of UNU Geothermal Training Programme, National Energy Authority of Iceland, Reykjavik, 88, 5

Pang Z (1991) Calibration of chemical geothermometers based on fluid-mineral equilibrium calculations with application to the hot spring areas in the south of Fujian Province, China. Geotherm Resour Counc Trans 15:273–278

Pang Z (1992) Theoretical calibration of chemical geothermometers and its application to the granitic geothermal areas of SE China. In: Kharaka YK, Maest AS (eds) Water-Rock Interaction, Balkema, pp 1463–1466

Pang Z, Armmannson H (1989) Modeling chemical equilibrium in hydrothermal systems: with examples from Iceland and China. In: Miles L (ed) Water-Rock Interaction, Balkema, pp 541–545

Pang Z-H, Reed M (1998) Theoretical chemical thermometry on geothermal waters: problems and methods. Geochim Cosmochim Acta 62(6):1083–1091

Pasvanoğlu S (2012) Hydrogeochemical study of the thermal and mineralized waters of the Banaz (Hamamboğazi) area, western Anatolia, Turkey. Environ Earth Sci 65(3):741–752

Piper AM (1944) A graphic procedure in the geochemical interpretation of water-analyses. EOS Trans Am Geophys Union 25(6):914–928

Reed M, Spycher N (1984) Calculation of pH and mineral equilibria in hydrothermal waters with application to geothermometry and studies of boiling and dilution. Geochim Cosmochim Acta 48(7):1479–1492

Reed M, Spycher N, Palandri J (2010) SOLVEQ-XPT: a computer program for computing aqueous-mineral-gas equilibria. University of Oregon, Department of Geological Sciences, Eugene, p 43

Roger F, Calassou S, Lancelot J, Malavieille J, Mattauer M, Zhiqin X, Ziwen H, Liwei H (1995) Miocene emplacement and deformation of the Konga Shan granite (Xianshui He fault zone, west Sichuan, China): geodynamic implications. Earth Planet Sci Lett 130(1):201–216

Royden LH, Burchfiel BC, van der Hilst RD (2008) The geological evolution of the Tibetan Plateau. Science 321(5892):1054–1058

Ryznar JW (1944) A new index for determining amount of calcium carbonate scale formed by a water. J Amer Water Works Ass 36:472–486

Scanlon BR, Healy RW, Cook PG (2002) Choosing appropriate techniques for quantifying groundwater recharge. Hydrogeol J 10(1):18–39

Schoeller H (1962) Les eaus souterrians Masson et. Cie, Paris

Shen L (2007) The study of deep source CO_2 degasification and carbon cycle in the southwest of China. Southwest University

Su B, Chen Y, Liu F, Wang Q, Zhang H, Lan Z (2006) Geochemical characteristics and significance of Triassic sandstones of Songpan–Ganzi block. Acta Petrol Sin 22(4):961–970

Tarcan G (2005) Mineral saturation and scaling tendencies of waters discharged from wells (>150 °C) in geothermal areas of Turkey. J Volcanol Geoth Res 142(3):263–283

Truesdell A (1976) Summary of section III geochemical techniques in exploration. In: Proceedings of the Second United Nations Symposium on the Development and Use of Geothermal Resources, San Francisco, pp 1iii-1xxix

Vengosh A, Helvacı C, Karamanderesi ISH (2002) Geochemical constraints for the origin of thermal waters from western Turkey. Appl Geochem 17(3):163–183

Wang E (1998) Late Cenozoic Xianshuihe–Xiaojiang, Red River, and Dali fault systems of southwestern Sichuan and central Yunnan. Geological Society of America, China

Wang Y, Liu S, Bian Q, Yan B, Liu X, Liu J, Wang H, Bu X (2015) Scaling analysis of geothermal well from Ganzi and Countermeasures for Anti-scale. Adv New Renew Energy 3(3):202–206

Wei M, Tian T, Sun Y, Li X (2012) A study of scaling trend of thermal groundwater in Kangding county of Sichuan. Hydrogeol Eng Geol 39(5):132–138

Xu G, Kamp PJ (2000) Tectonics and denudation adjacent to the Xianshuihe Fault, eastern Tibetan Plateau: constraints from fission track thermochronology. J Geophys Res Solid Earth 105(B8):19231–19251

Xu Z, Yang J, Li H, Ji S, Zhang Z, Liu Y (2011) On the tectonics of the India-Asia Collision. Acta Geol Sin 85(1):1–33

Yeh H-F, Lee C-H, Hsu K-C (2011) Oxygen and hydrogen isotopes for the characteristics of groundwater recharge: a case study from the Chih-Pen Creek basin, Taiwan. Environ Earth Sci 62(2):393–402

Zhang Y, Hao Z (1991) Regional geology of Sichuan Province. Geological Publishing House, Beijing

Zhang P-Z, Shen Z, Wang M, Gan W, Bürgmann R, Molnar P, Wang Q, Niu Z, Sun J, Wu J (2004) Continuous deformation of the Tibetan Plateau from global positioning system data. Geology 32(9):809–812

Zhang H, Hu Y, Yun Z, Qu Z (2016) Applying hydro-geochemistry simulating technology to sudy scaling of the high-temperature geochemical well in Kangding County. Adv New Renew Energy 4(2):111–117